Shelving of Barium Ion by Two Lasers Raman Transition

CHEN Zhanjiang

An academic exercise presented in partial fulfilment for the degree of Bachelor of Science with Honours in Physics.

Supervisor: Asst. Prof. BARRETT, Murray Douglas

Department of Physics

National University of Singapore

2009/2010

Acknowledgements

I would like to extend my word of thanks to all the members of the micro-trap group for the help rendered throughout the course of my project. It was definitely a great experience working with the group.

Many thanks to my supervisor Murray, who patiently guided and advised me throughout the project. It was a priviledge working with him.

I would also like to express my gratitude to Ting Rei, Boon Leng and Sarah, who assisted me in all aspects of the project.

Abstract

A laser system was developed that provides both 493 nm and 650 nm laser light suitable for addressing energy levels in singly ionized Barium. The relative frequency drift between the two lasers was measured to be < 1 MHz/hour with individual line-widths measured to be of the order of 1 kHz. These parameters make it possible to drive two photon Raman transitions between energy levels that are separated in frequency by many THz. In this thesis, we discuss the experimental setup and characterization of the laser system.

Contents

Chapter 1

Introduction

In many works done to attain the final goal of quantum computing, various quantum information systems are investigated and ion trap is one of the potential candidates for conveying the information via the state of the ions. In such a system it is necessary to provide the means to detect which state the ions are in to extract the information and this is often done using state sensitive florescence measurements.

In this work we consider the use of $^{137}Ba^{+}$. Barium ions have available transitions in the visible spectrum that makes it a particularly attractive for combining the ion trap system with cavity QED which would provide the means of exchanging information between ions and photons and ultimately providing an optical link between remotely located ions. However $^{137}Ba^{+}$ does not have a readily available cycling transition on which to base the required state-sensitive detection.

Consider the level structure given in Fig. 1.1. We want to have well defined internal states of Barium-137 for the purpose of quantum computing. Here we define the qubit as the hyperfine splitting of the $S_{1/2}$ ground state. The $S_{1/2}$ state has $F = 1$ and $F = 2$ sublevels, with spacing of 8037.742 MHz [1]. A three level system is formed with a 493nm transition from $S_{1/2}$ to $P_{1/2}$ and a

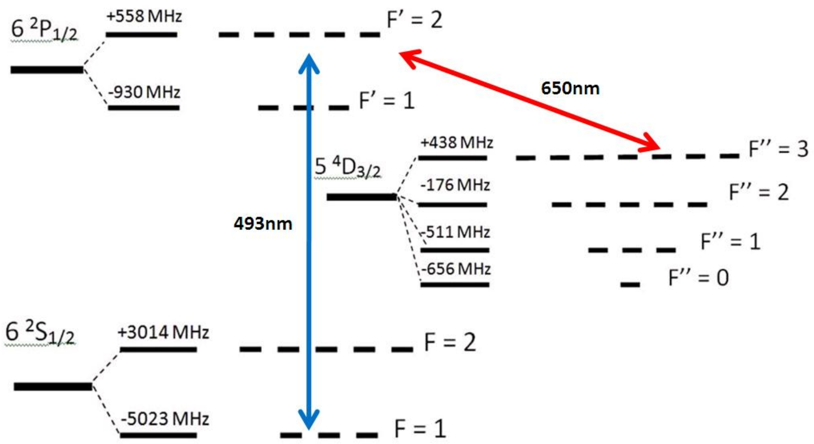

Figure 1.1: Energy level of Barium ion

650nm transition from $D_{3/2}$ to $P_{1/2}$. For convenience we denote the angular momentum of the S, P and D states to be F, F' and F'' respectively.

If the ion was in either the $|F = 1, M_F = 1\rangle$ or $|F = 2, M_F = 2\rangle$ state then driving transitions to the upper $F' = 1$ state would ultimately drive the ion into one of the $F'' = 0, 1,$ or 2 states of the $D_{3/2}$ state manifold. Since these states are long lived (30 s), fluorescence is only observed by using a repump laser at 650nm to pump the ion back into the $S_{1/2}$ state. The observed fluorescence then provides detection of the ion but not in a state selective manner. However if we first transfer population in the $|F = 1, M_F = 1\rangle$ to the $|F'' = 3, M''_F = 3\rangle$ level of the $D_{3/2}$ state manifold, fluorescence would only then occur if the ion started in the $|F = 2, M_F = 2\rangle$ state. Thus to provide state selective detection we require an efficient means to transfer population from the $|F = 1, M_F = 1\rangle$ ground state to the $|F'' = 3, M''_F = 3\rangle$ D-state.

In this thesis we describe the development of the laser system needed to provide the high efficiency population transfer discussed above. In Chapter 2, we discuss the theoretical considerations of two photon Raman transitions. These considerations highlight the difficulties faced when using lasers at very different wavelengths and indicates the experimental requirements that our laser system needs to achieve. In Chapter 3, we outline the experimental considerations involved in the design and the subsequent set up is descirbed in Chapter 4. In Chapter 5, we describe the characterization of the laser system. Finally in Chapter 6, we summarize our findings and outline future directions.

Chapter 2

Theoretical Considerations

In this chapter, we explore the requirements of the lasers required to carry out the shelving process. It is essential to understand that the efficiency of the shelving process directly links to the accuracy of the quantum readout for state detection. To understand how the various experimental factors affect the efficiency of the shelving process we model the system as a three level atom. Since the transfer is achieved via a Raman process with far detuned lasers, spontaneous emission can be neglected. Thus we start with an adiabatic elimination of the excited state to reduce the model to an effective two level atom. In doing so, we show that the main influences on the transfer process are the linewidth and relative detuning of the laser beams as well as the coupling of the lasers to the motional states of the ion. Simulations done elsewhere indicate that the detection efficiency is limited by off-resonant excitation from the $F'' = 3$ shelved state by the repumping light. This limits the detection efficiency to approximately 95%. Thus to ensure this limit is achieved we seek to achieve a shelving efficiency of 99% or better. From our effective two level model we are able to obtain estimates of the required frequency stability and level of laser cooling needed to obtain this efficiency. These estimates then serve as a guide for our experimental design.

2.1 An Effective Two Level Model

To obtain the requirements for the raman lasers to achieve coherent population transfer at an efficiency of 99%, we look at the three level system of the energy levels of Barium-137 (Refer Fig. 2.1). We choose to carry out the raman transition from $S_{1/2}$ to $D_{3/2}$ via a virtual state that is 80GHz red-detuned from $P_{1/2}$ state. This large detuning suggests that the $P_{1/2}$ state is almost never populated and we would be able to do an adiabatic elimination of the three level system to an effective two level system, involving only the $S_{1/2}$ and $D_{3/2}$ states.

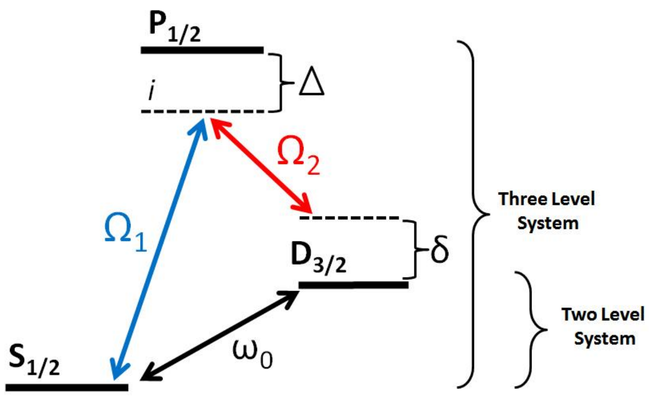

Figure 2.1: Reduction of three level system to effective two level system

After a reduction of the three level system to a two level system due to a large detuning from the excited state, the effective rabi flopping rate is given as follows

$$\Omega_R \propto \frac{\Omega_1\Omega_2}{\Delta} e^{i\left(-\Delta\omega t+\Delta\phi+\Delta\vec{k}\cdot\vec{x}\right)} \tag{2.1}$$

The $\Delta\omega t$ term in the exponential is accounted for in the two level model by the two photon detuning δ. The $\Delta\phi$ term describes the relative phase fluctuations of the lasers. In typical setups, the Raman lasers are derived from the same laser and it can be considered fixed. However it is not possible to easily achieve this in our system and the effects are accounted for in our model by the decay term γ, which is determined by the average laser linewidths [6]. The final $\vec{\Delta k} \cdot \vec{x}$ term determines the manner in which the external or vibrational states effect the laser couplings. This can be easily included by adding to the two level model a harmonic oscillator term to describe the external harmonic oscillator states. This makes the Raman transition rates depend on the motional states. For a mixture of motional states this diminishes the efficiency of the state transfer as discussed in section 2.4.

Since we are aiming to have each of these influences small, we consider them separately and neglect any possible interplay between them. We begin the analysis from the three level optical bloch equations. A detailed description for the excited state elimination is provided in Appendix B.

The elimination of the excited state yield the following results for the effective two level system, expressed in matrix form.

$$\frac{d}{dt}\begin{pmatrix}\rho_{11}\\ \rho_{22}\\ \rho_{12}\\ \rho_{21}\end{pmatrix} = \frac{i\Omega_R}{2}\begin{pmatrix}0 & 0 & 1 & -1\\ 0 & 0 & -1 & 1\\ 1 & -1 & \frac{2}{\Omega_R}(i\gamma-\delta) & 0\\ -1 & 1 & 0 & \frac{2}{\Omega_R}(i\gamma+\delta)\end{pmatrix}\begin{pmatrix}\rho_{11}\\ \rho_{22}\\ \rho_{12}\\ \rho_{21}\end{pmatrix} \tag{2.2}$$

Here, ρ_{ij} is the density operator. ρ_{11} and ρ_{22} represents the population of state 1 and 2, namely $S_{1/2}$ and $D_{3/2}$ states respectively. ρ_{12} is the coherence between the two states. Ω_R is the effective rabi flopping rate, which is calculated to be 2MHz using the beam parameters (refer Appendix A). δ is the absolute detuning of the laser beams from $S_{1/2}$ and $D_{3/2}$ states (refer Fig. 2.1). When $\delta = 0$, the raman transition is on resonance. γ is the average laser linewidth of the lasers.

In the following sections, we shall look at how the two variables, namely the absolute frequency detuning and laser linewidth, will affect the transfer efficiency of the shelving process.

2.2 Absolute Frequency Requirement

As we are doing a raman pulse to carry out a coherence transfer of ions from $|F = 1, M_F = 1\rangle$ to $|F'' = 3, M''_F = 3\rangle$ state, we require the difference in frequency of our raman lasers to coincide exactly with the energy difference of the states (i.e. ω_0) to ensure high transfer efficiency. This required frequency is also denoted as the absolute frequency requirement.

To understand the effects of a detuning (i.e. δ) from this absolute frequency, we set the average linewidth of the lasers $\gamma = 0$.

Using the bloch sphere picture, we define the following equations and Eq. 2.2 is expressed as a function of u, v and w.

$$\begin{aligned} u =& \rho_{11} - \rho_{22} \\ v =& i\left(\rho_{21} - \rho_{12}\right) \\ w =& \rho_{21} + \rho_{12} \end{aligned} \tag{2.3}$$

Solving for ρ_{22}, we obtain the following equation. A detailed solution would be provided in Appendix B.

$$\rho_{22} = \frac{1}{4}\frac{sin^2\left(\frac{\sqrt{1+\beta^2}}{2}\Omega_R t\right)}{\frac{1+\beta^2}{4}} \tag{2.4}$$

Here, we have defined $\beta = \frac{\delta}{\Omega_R}$. We want to solve for $\rho_{22} = 0.99$, which translate to a 99% transfer efficiency of the raman transition. We input parameters relating to a π-pulse and we obtain a solution of $\beta = 0.100$ (refer Fig. 2.2). This means that the absolute frequency fluctuation have to be within 10% of the raman rate to achieve 99% transfer efficiency. With the rabi flopping rate at 2MHz, this implies that we require the absolute frequency to be within 200kHz over the

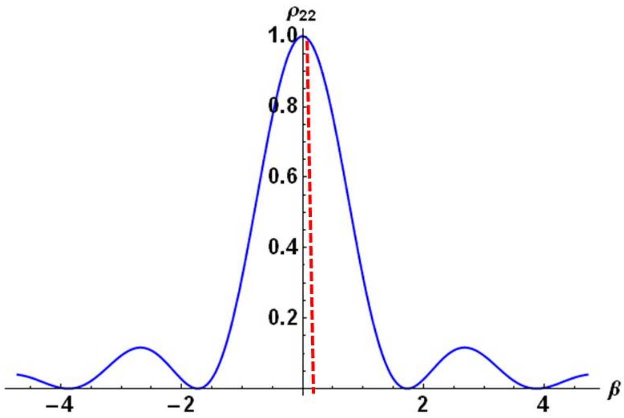

Figure 2.2: Graphical representation of Eq. 2.4. Graph is plotted with $\Omega_R t = \pi$. Solution of ρ_{22} yields $\beta = 0.100$.

experiment.

2.3 Phase Fluctuations

Our lasers are being produced from two different sources, therefore, there would be some inherent phase difference between the lasers that could not be eliminated. This decoherence in the raman beams would decrease the population transfer efficiency. We can view this phase fluctuation as a fast frequency jitter in the laser beams, which corresponds to the linewidth of the lasers. In a similar treatment as the previous section, we set the absolute frequency detuning $\delta = 0$ to understand the effects of the laser linewidths on the transfer efficiency. We also express Eq. 2.2 via the bloch sphere picture, simplifying expression via Eq. 2.3.

Solving for ρ_{22}, we obtain the following expression.

$$\rho_{22} = \frac{1}{2}\left(1 - e^{-\frac{\alpha\tau}{2}} cos\left(\sqrt{1 - \frac{\alpha^2}{4}}\Omega_R t\right)\right) \tag{2.5}$$

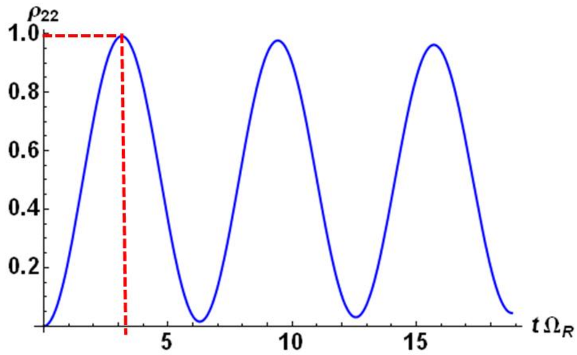

Figure 2.3: Graphical representation of Eq. 2.5. Eq. 2.5 is being solved for $\alpha = 0.99$ via a π-pulse. Solution of ρ_{22} yields $\alpha = 0.0128$.

In an absence of laser linewidth, the exponential term in Eq. 2.5 will drop out and the population of ions will simply oscillate between both the states. However, this phase fluctuations here causes a reduction in the efficiency of rabi flopping rate and the system will eventually reach an equilibrium where there is an equal chance of populating both states (i.e. $\rho_{22} = \rho_{11} = 0.5$) Here, we have defined $\alpha = \frac{\gamma}{\Omega_R}$. Similarly, we want to solve for $\rho_{22} = 0.99$, $\Omega_R t = \pi$ since we want a 99% transfer efficiency using a π-pulse. A solution to the equation would yield $\alpha = 0.0128$, which means that the average laser linewidth has to be about 1% of the raman rate, thus the laser linewdith of both lasers are required to be less than 20kHz.

2.4 Motional Coupling

The exponential term $\Delta k \cdot x$ can be expressed in terms of the ladder operators for the external harmonic potential which gives

$$\Delta k \cdot x = \eta(a + a^\dagger) \tag{2.6}$$

where η is the Lamb-Dicke parameter given by

$$\eta = \frac{1}{\sqrt{2}}\left(\frac{2\pi}{\lambda_{493}} - \frac{2\pi}{650}\right)\sqrt{\frac{\hbar}{2m\omega_T}} \tag{2.7}$$

ω_T is the trap frequency of the Linear Paul trap along the trap axis and the factor of $\frac{1}{\sqrt{2}}$ arises from the raman beams propogating at 45^o to the trap axis. The raman beams are considered to be propogating along the same direction, minimising the $\vec{\Delta k}$ term.

With this term the transition rate between internal states now depends on the external state. The transition rate from $n \rightarrow n$ is given by [4]

$$\Omega_n \equiv \Omega_R e^{\eta^2/2} L_n\left(\eta^2\right) \tag{2.8}$$

where $L_n\left(\eta^2\right)$ is a Laguerre polynomial. If we neglect off-resonant transitions between different vibrational states we can calculate analytically the effect of a thermal mixture of vibrational states. In this case the vibrational state is a mixture of n states with the probability of being in the n^{th} state given by

$$P_n = \frac{\bar{n}^n}{(1+\bar{n})^{n+1}} \tag{2.9}$$

where $\bar{n}$ is the average vibrational quantum number. The Raman beams then evolve the state according to

$$\begin{aligned} P\left(|2\rangle\right) &= \sum_{n=0}^{\infty} c_n^2 \sin^2 \frac{\Omega_{nn} t}{2} \\ &= \sum_{n=0}^{\infty} \frac{\overline{n}^n}{\left(1+\overline{n}\right)^{n+1}} \sin^2\left[\frac{\Omega_R t}{2}\left[1-\left(n+\frac{1}{2}\right)\eta^2\right]\right] \end{aligned} \tag{2.10}$$

Taking the pulse time to be the usual π, $\Omega_R t = \pi$, we can expand the Sine term to second order in η and we find

$$P\left(|2\rangle\right) = 1 - \frac{\pi^2}{4}\left(\bar{n}^2 + \bar{n} + \frac{1}{8}\right)\eta^4 \tag{2.11}$$

Here, the mean vibrational state can be estimated by the Doppler limits. The decay rate of the excited state is about 20MHz and a trapping frequency of about 200kHz is considered.

$$\begin{aligned} \overline{n} =& \frac{\Gamma}{2\omega_T} \\ =& \frac{20MHz}{2 \times 200kHz} \\ =& 50 \end{aligned} \tag{2.12}$$

Given a trap frequency of $\omega_T = 2\pi \times 200kHz$, we obtain $\eta \approx 0.03$. Considering a π-pulse, $\Omega_R t = \pi$, Eq. 2.11 can be evaluated numerically. With the above conditions, the transfer efficiency of the raman lasers is found to be $P\left(|2\rangle\right) = 0.99$. It is worthwhile to note that the transfer efficiency increases rapidly with a higher trap frequency since both $\bar{n}^2, \eta^4 \propto \frac{1}{\omega_T^2}$. This means that we can effectively suppress the effect of motional states with a well confined trap.

This gives us convincing results that the coupling to the vibrational modes of the ion will not affect the transfer efficiency of the shelving process significantly. It should be noted that it is not strictly valid to neglect the off-resonant coupling to other vibrational states particularly for the trapping frequency used here and the expected value of Ω_R. However the effect is only important at high values of n and is strongly diminished for higher trap frequencies. Thus we expect this to be only a correction to the analysis done here and not significantly alter the conclusion.

Chapter 3

Experimental Considerations

To achieve the requirements laid out in the previous chapter so as to obtain a high transfer efficiency for the raman lasers, various techniques were considered. Both the 650nm and 493nm lasers are locked to the same optical cavity. Since the drift of the resonance of the cavity can be correlated to the drift in the absolute frequency difference of the lasers, a 780nm laser is used to monitor the drift of the cavity. Methods that are used to increase the stability of the cavity will be discussed in section 3.1. The optical cavity used here have a mirror curvature of 5cm and a length of 10cm.

The laser linewidth of the 650nm free running diode laser is narrowed through an external cavity feedback method and both lasers are locked to the same cavity using the Pound Drever Hall technique. Further details will be discussed in section 3.2.

3.1 Cavity Stability

In order to maintain the absolute frequency difference detuning to less than 200kHz as mentioned in Chapter 2.2, we need to look into means of maintaining the difference in the frequencies between both 650nm and 493nm lasers. In other words, the frequencies of the lasers are allowed to fluctuate as long as the difference in their frequencies are within 200kHz of the energy level between $|F = 1, M_F = 1\rangle$ and $|F'' = 3, M_F'' = 3\rangle$. In order to achieve this, we couple both the lasers to the same cavity (refer Fig. 3.1), and the cavity is being stabilised to ensure minimal fluctuations to the laser frequencies.

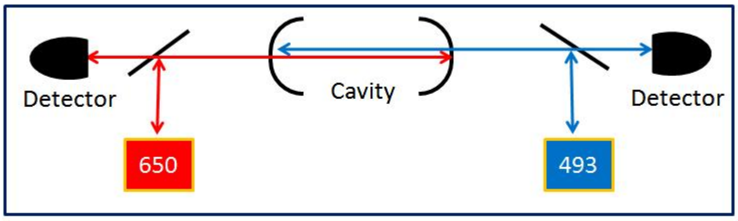

Figure 3.1: Both lasers are coupled to the same cavity and their frequencies are being monitored. Any drift in frequency of one laser would correspond to a correlated amount of drift in the other laser, thus allowing us to know the drift in the absolute frequency. It should be noted here that the actual frequency (for the blue laser) that is being coupled into the cavity is 986nm. 493nm is derived from 986nm after going through a second harmonic generation.

The cavity here acts as a frequency selection. The free spectral range of the cavity is given by

$$FSR = \frac{c}{2nL} \tag{3.1}$$

where, c is the speed of light, n is the refractive index of the medium and L is the cavity length. Any changes to the refractive index or the physical length of cavity would result in a change in the free spectral range of the cavity, therefore changing the frequency of the lasers locked to the cavity by different amounts.

This method allows us to monitor the drift in the absolute frequency difference by simply observing one cavity. Any drift in laser frequencies resulting from the change in optical path length of the cavity could be correlated to each other since both the lasers are coupled to the same cavity. Therefore, we could easily alter the laser frequencies as required to maintain high transfer efficiency.

3.1.1 780nm Laser As Reference

A laser of wavelength 780nm could be used as a reference to monitor the drift in the cavity once it has been set up. The 780nm laser could be locked to an atomic transition in rubidium and coupled into the cavity. Since there would not be any drift in frequency due to the laser source, any drift in frequency in the transmission signal would be due to the drift of the cavity.

The condition for resonance in the cavity can be viewed as the optical path length of the cavity, being an integer number of multiples of half the laser wavelengths. This gives rise to the following condition since all the lasers are coupled to the same cavity. It is important to note at this point that 650nm and 986nm lasers are coupled to the same cavity, while the 493nm laser is derived by frequency doubling the 986nm laser.

$$nL = n_{ref}\frac{\lambda_{ref}}{2} = n_R\frac{\lambda_R}{2} = n_B\frac{\lambda_B}{2} \tag{3.2}$$

where $n_{ref,R,B}$ refers to an integer of half wavelengths of 780nm, 650nm and 986nm lasers respectively. $\lambda_{ref,R,B}$ refers to the wavelength of 780nm, 650nm and 986nm respectively. L is the physical length of the cavity.

The absolute frequency can be expressed as

$$\begin{aligned} f_{abs} =& 2f_B - f_R \\ =& \frac{c}{2L}\left(2n_B - n_R\right) \end{aligned} \tag{3.3}$$

To understand the effect of the change in length of the cavity on frequency, we take the derivative of Eq. 3.3 with respect to L

$$df_{abs} = -\frac{c}{2L^2}\left(dL\right)\left(2n_B - n_R\right) \tag{3.4}$$

For any fluctuation in the physical length of the cavity, the change in frequency of the transmission signal from the cavity, f_c is given by Eq. 3.5. Here we assume that the refractive index, n, of the medium is close to unity. The change in frequency of the cavity would therefore be the change in length of the cavity expressed as a fraction of half the wavelength of the coupled laser, multiplied by the free spectral range.

$$df_c = \frac{dL}{\lambda/2} \times \frac{c}{2L} \tag{3.5}$$

Putting Eq. 3.5 into Eq. 3.4, the absolute frequency fluctuation can be expressed as a function of the drift of the cavity when observed with a 780nm laser as reference.

$$\begin{aligned} df_{abs} =& -\frac{\lambda_{ref}}{2L}\left(df_c\right)\left(2n_B - n_R\right) \\ =& -df_c\left(\frac{2n_B - n_R}{n_{ref}}\right) \\ \approx& 0.38 \times df_c \end{aligned} \tag{3.6}$$

Therefore, through understanding the drift in the transmission signal of the 780nm laser, which translate to the drift of the cavity over time, we would be able to know the approximate drift in the absolute frequency over the experiment. In order to achieve the 200kHz absolute frequency stability over the duration of the experiment, we would require our cavity to achieve the stability of about 1MHz over an hour. This implies that we need to monitor the absolute frequency difference every half an hour and recalibrate the laser frequencies if neccessary.

Stabilising the cavity that both lasers are coupled to would make the job much easier as the drift in laser frequencies would be reduced significantly. We look into means of stabilising the optical path length of the cavity in the next few sections.

3.1.2 Dependence of Optical Path Length on Temperature

The optical path length of the cavity is given by [3]

$$L_{optical} = n_{medium} \times L_{cavity} \tag{3.7}$$

where n_{medium} is the refractive index of the medium inside the cavity and this value is assumed to be the same over the length of the cavity. L_{cavity} is the physical length of the cavity. Let us first investigate the dependence of the refractive index of the medium on temperature. In the following argument, we assume that the laboratory pressure is stabilised at 101325 Pa, and calculations are based on the laboratory temperature of 22^oC.

The refractive index of standard air (defined as dry air at 15^oC, 101325 Pa, containing 0.045% by volume of carbon dioxide) is given by

$$n_s = 1 + 0.0472326 \times \left(173.3 - \sigma^2\right)^{-1} \tag{3.8}$$

where σ is defined as follows in $(\mu m)^{-1}$

$$\sigma = 1/\lambda_{vac} \tag{3.9}$$

For air at temperature T^oC, and pressure P, the refractive index is given by

$$n_T = (n_s - 1) \times \frac{P\left(1 + P\,(60.1 - 0.972T) \times 10^{-10}\right)}{96095.43\,(1 + 0.003661T)} \tag{3.10}$$

Based on the laboratory temperature of 22^oC, $P = 101325Pa$, the refractive index of air is found to be 1.00027. By taking the first derivative of n_T with respect to temperature, the rate of change of the refractive index of air can be found. For every degree change in laboratory temperature

$$\Delta n \approx -2 \times 10^{-5} \tag{3.11}$$

Therefore, for every degree change, the optical path length of the cavity would change by

$$\begin{aligned} \Delta L_{optical} &= \frac{\Delta n}{n} \times L_{optical} \\ &\approx 2 \times 10^{-6} m \end{aligned} \tag{3.12}$$

Let us assume that the physical length of the cavity is constant. The change in resonance frequency of the cavity due to the change in the refractive index of the medium is the change in the optical length of the cavity expressed as a fraction of half the wavelength of the coupled laser, multiplied by the free spectral range

$$df_c = \frac{d\,(nL)}{\lambda/2} \times \frac{c}{2nL} \tag{3.13}$$

The change in the optical path length per degree change in temperature is of the order 10^{-6}m, which is an order larger than the wavelength of the visible light. The change in the absolute frequency of the laser coupled to the cavity would fluctuate in the order of 1 GHz (from Eq. 3.6) and this implies that for every degree change in laboratory temperature, the raman transfer efficiency would sharply decreased. This problem could be eliminated by putting the cavity in a vacuum chamber, thus maintaining the refractive index of the medium constant ($n_{medium} \approx 1$). This thermally isolates the cavity from the environment.

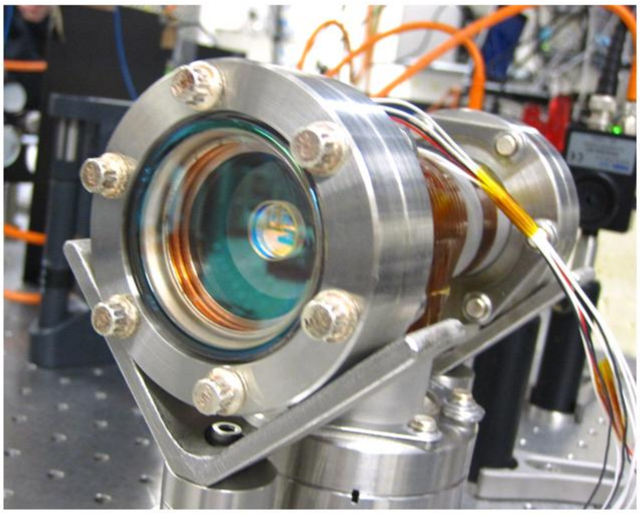

Figure 3.2: The cavity mirrors is held by a hollow tube made of Zerodur. It is then placed in the vacuum chamber, sitting on rubber rings as insulation and isolation from conduction. The chamber is estimated to be pumped down to 10^{-4}Torr.

To ensure that the physical length of the cavity does not exhibit large fluctuation, the material used for the construction of the cavity is chosen to exhibit minimal response to its surroundings. The cavity mirrors are mounted on the ends of a hollow tube, which acts as a support that maintains the position of the mirrors. The material chosen for this tube is Zerodur, which has an expansion coefficient of (0.00 ± 0.02)ppm/K [12]. This would ensure that the physical length of the cavity does not respond significantly to any drift in laboratory temperature.

The cavity sits on rubber rings inside the vacuum chamber. The rubber spacers acts as a support to prevent conduction from the vacuum chamber to the cavity (refer Fig. 3.2). They also aid to isolate the cavity from vibrations. The chamber is then pumped down by means of a mechanical pump for one day, followed by another day of bake out. It is estimated to be pumped down to about 10^{-4}Torr.

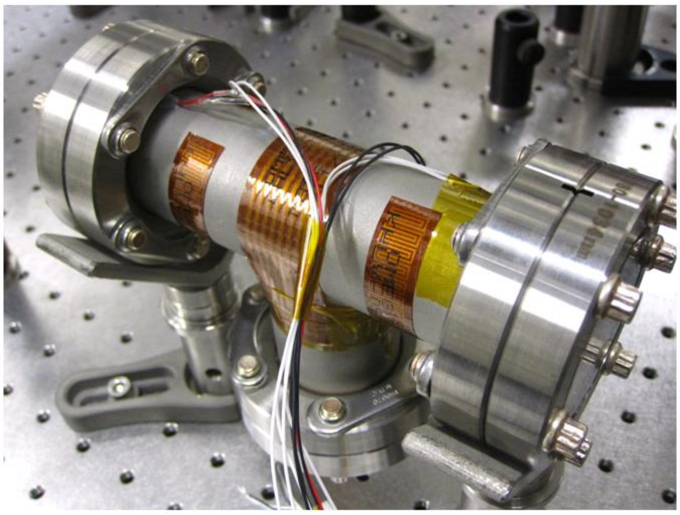

Figure 3.3: The heating strips are resistors that dissipate heat upon passing through a current. The strips are stuck on the vacuum chamber to temperature stabilise the chamber, taking out the slow drift of the laboratory temperature over the day.

To further minimise the effects of the drift of temperature in the laboratory on the change in optical path length of the cavity, we look further into isolating the vacuum chamber from the surrounding. Heating strips are attached to the vacuum chamber (refer Fig. 3.3) and the chamber is heated up to about 27^oC. This equilibrium temperature is chosen to be slightly above normal laboratory temperature of 22^oC, so that any drifts in the laboratory temperature could be compensated by the heating strips as the strips come to a thermal equilibrium with the surroundings. The heating strips are expected to take out the slow drift in the laboratory temperature over the day. The vacuum chamber is then wrapped up with aluminium foil to ensure even heating over the whole surface of the chamber.

The cavity with the heating strips is then placed inside a box. The vacuum windows are insulated from the surrounding by putting on a plastic cap. The plastic cap is constructed with only a small hole in the centre to allow the laser to pass though. This is to reduce the effect of

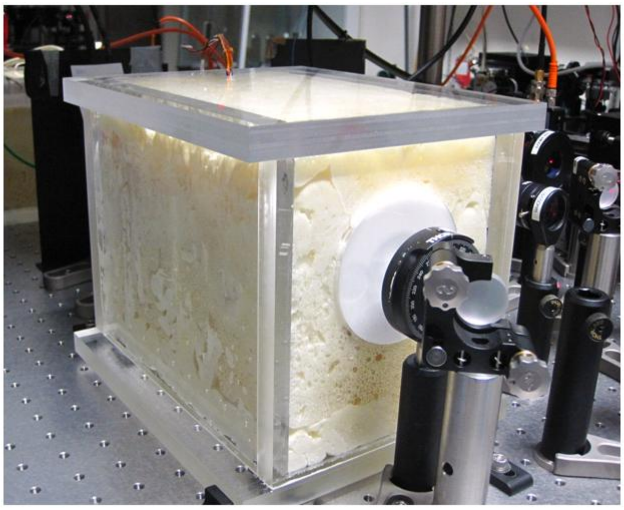

Figure 3.4: The cavity is placed in a box and filled up with insulating foam. The vacuum windows are insulated from the surrounding to reduce radiation from the metal windows. This is targeted to take out the fast drift of the laboratory temperature.

radiation from the exposed area of the vacuum window due to huge temperature difference that could suddenly occur. This method has proven to be helpful in increasing the stability of the cavity in an initial prototype when a piece of foam was put over the vacuum window to act as a shield. The box is then filled up with insulating foam (refer Fig. 3.4). Great Stuff^{TM} sealing foam is used here. It uses polyurethane, which expands upon curing in air. This allows us to effectively seal up the vacuum chamber inside the box and insulate it from the surrounding despite its irregular shape.

3.2 Cavity Locking

In order to achieve the linewidth requirement of the lasers to be less than 20kHz, we employ the technique of external cavity feedback to narrow the linewidth of our 650nm laser [8]. Diode lasers are known to have very poor linewidth of more than 10MHz [9], therefore the external cavity feedback method is used to narrow the linewidth of the 650nm laser.

3.2.1 External Cavity Feedback

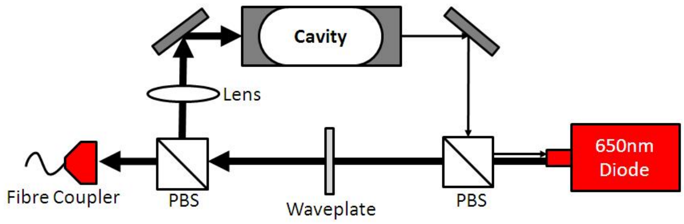

Figure 3.5: Schematic of the feedback system for the external cavity for 650nm laser. Laser from the 650nm diode is coupled to the cavity and the transmission signal is feedbacked to the diode.

The 650nm laser is coupled to the very same cavity used to stabilise the frequency of the laser in the previous section. This cavity acts as a filter (on top of being a frequency selection) here and it only allows a narrow range of frequency to pass through.

There has been many works done about the cavity mode that the laser should be coupled to for the external cavity feedback method. Many of which mentioned about a confocal cavity coupled with the TEM 00 mode, being slightly tilted such that the cavity sets up a resonance with a 'V' shape mode. The reflected transmission signal from the cavity is then feedbacked to the diode [9] [10]. However, several issues were encountered with this method. Firstly, it was very hard to determine whether we had achieve the 'V' shape mode that was required. Much effort was spent using various techniques before the 'V' shape condition was believed to have been achieved. However, the feedback to the laser diode was not optimum and there were much noise in the feedback. This affected the stability of laser and the laser could not stay lock for more than five minutes.

Since the fundamental idea behind this technique is to use the cavity as some sort of frequency filter, we feedback the transmission signal (though the cavity) instead. The noise in the transmission signal is much lower and by passing the feedback signal through a PBS and an optical isolator, the signal from the feedback is much cleaner and the stability of the lock for the laser increases.

With the appropriate optical geometry, the laser optically self-locks to the resonance of the cavity. The linewidth of the tunable diode is effectively narrowed.

3.2.2 PDH Locking Technique

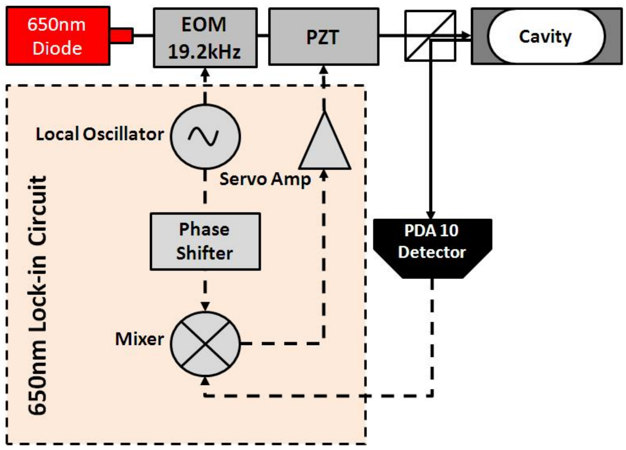

Figure 3.6: Schematic of the lock in circuit for the PDH lock of the laser. The reflected signal from the cavity is picked up by the photodetector and demodulated with the local oscillator signal via the mixer. The board then controls the output to the PZT to keep the laser on lock.

The laser is locked mechanically using the Pound-Drever-Hall technique. Sidebands of 19.2kHz are put onto the laser by an Electric Optic Modulator (EOM). When the laser is on resonance with the cavity, the 19.2kHz sidebands will be off resonance and be reflected back by the cavity. This reflected signal of the sidebands is then picked up by a high bandwidth detector from Thorlab, PDA10. The intensity of the signal observed by the detector is fed to a lock-in circuit board, where the signal will be demodulated with the local oscillator via a mixer (refer Fig. 3.6). An antisymmetric error signal would be generated.

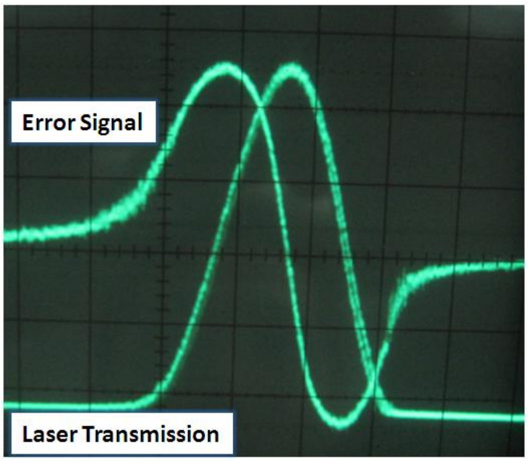

Figure 3.7: Antisymmetric error signal used for locking of laser to a resonance of the cavity transmission.

Any drifts in the laser frequency would result in the decrease in the intensity of the transmission signal. However, the transmission signal is not used here for the locking of laser because of its symmetric property. It is noted that an increase or decrease in frequency would both result in a decrease in the transmission intensity. On the contrary, the error signal generated is an antisymmetric function. The resonance of the cavity transmission corresponds to a zero level in the error signal. The gradient of the transmission signal corresponds to the polarity of the error signal, thus the direction of change of the frequency of the laser could be understood through the polarity of the error signal. The board then controls how much voltage would be applied to the PZT driver and the actuator, which changes the round trip phase of the laser so that the laser stays on resonance with the cavity [11].

3.2.3 High Finesse Cavity

The laser line-widths we obtained are much lower than anything else available. Thus a special high finesse cavity, that had a line-width of approximately 50kHz at both 493nm and 650nm, was used in order characterize the frequency noise of the lasers. This high finesse cavity has mirrors of radius 5.0cm and the cavity length of 4.87cm. The mirrors are coated for 650nm and 493nm. A detailed discussion on the characterisation and the measurement of the the linewidth of the cavity and the lasers would be provided in Chapter 5.

Chapter 4

Equipment Setup

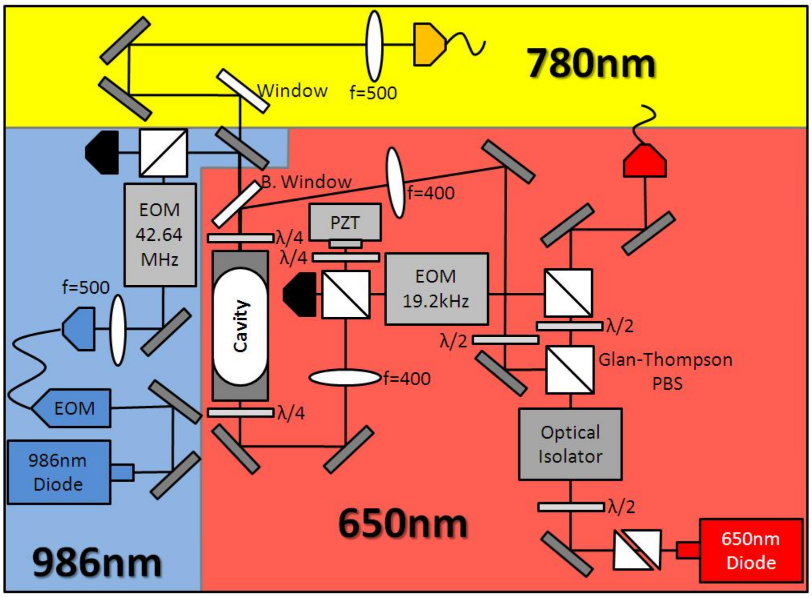

Figure 4.1: Simplified schematic of the setup of the lasers. 650nm and 986nm lasers are coupled to the cavity at the same time for the experiment. 780nm laser is used as a reference to monitor the drift in the frequency of the cavity.

The laser setup for the experiment allows 650nm and 986nm raman lasers to be coupled and locked to the same cavity at the same time. 780nm laser, which acts as an reference, could also be allowed access to the cavity without disrupting the setup for the other two lasers. Methods to construct and integrate the setup together will be described in the following sections.

4.1 650nm Setup

The 650nm setup comprises mainly of the laser diode, the cavity for the external cavity feedback system and the setup for the locking system. Each component will be analysed below.

4.1.1 Laser Diode and Housing

The 650nm laser is produced from a free running diode that operates at about 654nm at room temperature (22^oC). In order to achieve the required wavelength of 650nm, the diode is cooled down to about -15^oC using a thermo-electric cooler (TEC). Initially, a high power diode laser that produces about 9.0W at 28mA was used. However, the laser produced at room temperature was found to be 659nm. Cooling down to -15^oC only manages to increase the frequency of the laser to about 654nm, which is far from favourable, therefore the experiment now uses the lower power diode which produces about 6.0W at 28mA.

To prevent water from freezing and crystallising on the diode, which would then affect the laser profile, the air inside the diode housing is pumped out via a mechanical pump and dry nitrogen gas is leaked into the housing simultaneously. Desiccants are put inside the housing to ensure no formation of water crystals on the diode. The TEC is attached to the housing that holds the diode. The other end of the TEC is attached to a heat sink with fins for dissipation of heat. The TEC is controlled by a temperature controller circuit board that dumps heat from the laser housing to the heat sink, based on a set point on the circuit board that can be manually changed.

Due to the large temperature difference between the laboratory temperature (22^oC) and the temperature set point of the laser (-15^oC), large amount of heat is dumped into the heat sink and the heat has to be dissipated fast. A 12V cooler fan is placed near the heat sink with fins to aid in the dissipation of heat. Previous attempts to dissipate the heat from the diode housing via methods such as heat pipes and heat sink with fins have failed, which could be attributed to the slow rate of heat dissipation that the methods provide. This will increase the temperature gradient across the TEC, resulting in the current supply to the TEC to slowly increase, so as to maintain the temperature of the diode. The ineffective cooling of the TEC results in the TEC being unable to maintain the diode at the required temperature.

Initially, the cooler fan introduced caused vibrations on the optical table that it sits on and introduced unwanted air flow towards the setup. The quality of the feedback signal fluctuate wildly, affecting the stability of the lock. To reduce the effect of the vibrations of the fan, the cooler fan is made to sit on rubber dampers. Care is also taken to ensure that the fan does not direct the air current towards the rest of the setup due to the nature of the external cavity feedback technique, which is extremely sensitive to any mechanical noise. On top of that, the laser housing is placed slightly further away from the setup to minimise mechanical noise.

The laser that exits the housing is set to be vertically polarised and the beam profile is slightly elliptical. The beam first passes through an anamorphic prism pairs of magnification 3.5 to obtain a circular beam. The vertically polarised laser is then passed through a half-waveplate that rotates the linear polarisation of the laser to about 45^o. It is then passed through an optical isolator, which is effectively a faraday rotator, which rotates the polarisation of the beam by 45^o, obtaining an output of horizontal polarisation. Here, the beam meets a Glan-Thompson polariser beam splitter that allows most of the light to pass through. Another half-waveplate after the polariser beam splitter rotates the horizontally polarised beam to a desired angle. This half-waveplate controls the intensity of the beam that goes towards the cavity. Right after the half-waveplate, there is a polarising beam splitter (PBS) that directs vertically polarised light towards the cavity and transmits the horizontally polarised light to a fibre coupler. Depending on how much power is required to be coupled into the cavity for the feedback technique to be working at the optimum, the half-waveplate could be manipulated to achieve the desired conditions. The laser that is coupled to the fibre would be used for the experiment.

4.1.2 Electric Optic Modulator

The vertically polarised laser that is reflected by the PBS passes through an in-house constructed electric optic modulator (EOM) of resonant frequency 19.2MHz. The EOM is basically a nonlinear crystal that allows its refractive index in certain directions to be changed by the application of an electric field. The laser is then phase modulated by the EOM and sidebands of ±19.2MHz are formed.

4.1.3 Piezo

The laser then hits a PBS that reflects almost all the power towards a piezoelectric material, Lead Zirconate Titanate (PZT), which is mounted on a piezoelectric actuator. A piezoelectric material is able to produce a stress/ strain on the material upon application of an electric field. This means that the 'thickness' of the material could be controlled by the amount of voltage applied. The change in the 'thickness' would then effectively change the pathlength of the laser. The PZT used has an effective response of $4\mu m$ over 100V while the actuator is able to produce effective movements of up to $80\mu m$ over 75V. The PZT and the actuator are used for locking of the 650nm

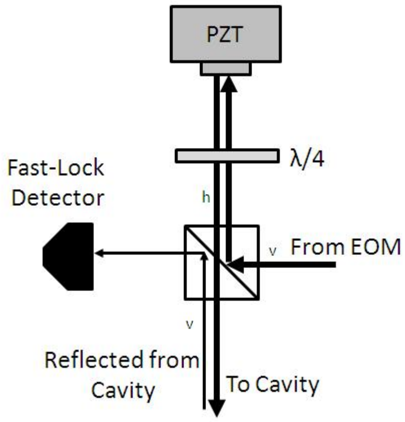

Figure 4.2: 650nm laser hits the PBS with a vertical polarisation and is reflected towards the PZT with a mounted mirror. The laser double passes the quarter-waveplate, changing the polarisation to horizontal and is transmitted by the PBS. Reflected signal from the cavity is vertical due to double passing of another quarter-waveplate, reflecting at the PBS towards the fast-lock detector.

laser (refer section 3.2). The PZT is used to track the fast drift of the laser frequency while the actuator which has a larger response is able to keep the laser locked for long period of time.

A small mirror is mounted on top of the PZT, and it reflects the laser back towards the PBS. A quarter-waveplate is placed in between the PBS and the PZT to change the polarisation of the laser from vertical to horizontal (due to double pass of quater-waveplate). The horizontally polarised laser is then passed through the PBS (refer Fig. 4.2) and coupled into the cavity via a lens with focal length of $f = 400$mm.

PZT Geometry

The initial setup uses the mirror on the PZT to direct the laser towards the cavity as shown in Fig. 4.3. In such a setup, the change in path length of the laser would be a factor of $\sqrt{2}$ greater than the movement of the PZT. This is because the laser hits the mirror on the PZT at an angle of 45^o. However, this method produced an unexpected large deviation in the coupling of the laser to the cavity. As demonstrated in Fig. 4.3, the movement in the PZT can effectively change the geometry at which the laser hits the mirrors and enters the cavity, therefore changing the coupling. It can be seen on the transmission signal of the cavity that the intensity of the resonance over a range of scanning in the PZT decreases. Changing the orientation of the mirrors during scanning slightly aids in improving the signal, implying that the scanning of the PZT is affecting the coupling of the laser to the cavity.

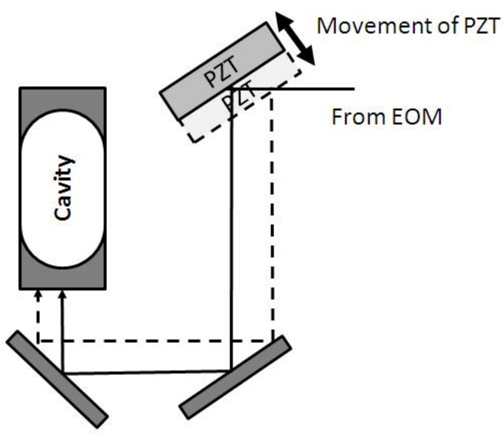

Figure 4.3: The initial setup of the PZT is at an angle of 45^o and by the geometry of the set up, it causes the coupling of the laser to the cavity to be changed. The diagram is exaggerated to illustrate the effects of the movements of the PZT on the coupling.

To rectify this problem, the set up was changed to that of Fig. 4.2. In this method, the geometry of the laser entering the cavity is not affected by any movements from the PZT. The laser is hitting the mirror on the PZT at normal incidence. This method also serves to improve the effective working range of the PZT. Instead of changing the path length of the laser by a factor of $\sqrt{2}$ in the initial setup, the path length of the laser is changed by a factor of 2 here since the laser is hitting the mirror at normal incidence (and reflected back). This means that for every movement in the PZT, it would be able to change the path length of the laser over a larger range, so as to compensate for any drifts in the laser frequency, or the length of the cavity.

4.1.4 Coupling to Cavity and Feedback to Diode

The laser is coupled into the TEM 00 mode in the cavity. Quarter-waveplates at both ends of the cavity changes the polarisation of the outgoing beam (from the cavity) from horizontal to vertical. The window is then set to be at brewster angle to minimise any unwanted polarisation. This is essential as the transmission signal from the cavity is feedbacked to the diode laser and only a clean signal from the cavity would ensure desired feedback effects. In order to determine the brewster angle for this signal, we first attempt to produce horizontally polarised light at the window by simply flipping the latter quarter-waveplate. Thereafter, the reflected signal from the window is minimised, implying that the window is at brewster angle since only vertically polarised light is reflected at brewster angle. The quarter-waveplate is then flipped back to the original configuration to produce horizontally polarised light. About 2% of the power of the 650nm laser is reflected by the window at Brewster angle for the feedback while 98% is transmitted to a photodetector. The light is then directed back towards the diode laser via the Glan-Thompson beam splitter. A half-waveplate is placed before the mirror to control the amount of power that is feedbacked into the cavity.

To ensure that the transmission signal is well feedbacked to the diode, the 'stray' beam that is initially deflected by the Glan-Thompson beam splitter is used. This beam is being coupled into the the cavity into the TEM 00 mode through the 'rear' of the cavity. The fact that both the 'stray' beam and the feedback signal are taking the same path, a well coupled stray beam to the cavity would imply that feedback signal is well coupled back into the laser diode.

The laser is locked using the Pound-Drever-Hall technique. When the laser is on resonance with the cavity, the 19.2kHz sidebands that are generated by the Electric Optic Modulator will be off resonance and be reflected back by the cavity. This reflected signal of the sideband is then reflected by the PBS (refer Fig. 4.2) to a high bandwidth detector from Thorlab, PDA10.

4.2 986nm Setup

The 986nm laser system was commercially purchased from Toptica. The system consists mainly of two components, the 986nm diode setup with a high bandwidth electronic locking system, and a frequency doubling system by second harmonic generation. Laser produced by the 986nm diode is split into two paths, one for producing the 493nm laser and the other for locking of laser. The 986nm laser is frequency doubled by a non-linear crystal to produce 493nm laser in one of the paths. As for the other path, it is coupled into a EOSPACE EOM (thereafter mentioned as EEOM in the document). It is a wideband phase modulator that is coupled to an optic fibre. The modulation to the laser frequency is tunable via a signal generator that supplies the RF output to the EOM.

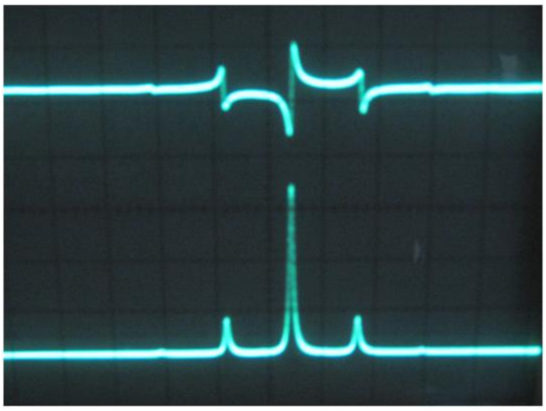

Figure 4.4: The signal above shows the error signal generated. The signal below shows the transmission signal (of the sideband generated by EEOM) of the 986nm laser. Further sidebands have been put on the 986nm laser by an EOM of 42.64MHz and can be seen from the signal below. The laser is locked to the peak, which corresponds to the middle of the slope of the error signal.

The output of the laser from 780nm compatible EEOM is then passed through an EOM of resonance frequency 42.64MHz and thereafter coupled into the cavity as shown in Fig. 4.1. Here the mirrors used are coated for 986nm laser and at an angle of 45^o, the transmission of 650nm and 780nm through the 986nm mirror is about 90% and 75% respectively. This allows the 986nm laser to be coupled into cavity while allowing optical access for 650nm and 780nm. The EEOM allows the signal generator to put sidebands on the laser frequency. This frequency of the sidebands are tunable by the signal generator and would be adjusted to attain the required absolute frequency. The 42.64MHz EOM then further puts sidebands on the signal from EEOM to lock the laser to the sideband of EEOM. The 986nm laser is locked in a similar fashion as that for 650nm laser using the PDH technique. The reflected signal of the sidebands are demodulated and the error signal is generated (Refer Fig. 4.4). The laser is locked to the peak of the transmission, which corresponds to the zero intensity level of the error signal (at the middle of the slope). Slow adjustments to the frequency of the sidebands from EEOM could be followed by the PDH lock, therefore allowing slow scanning of laser frequency while maintaining the lock of the laser.

4.3 780nm Setup

The 780nm laser is a grating stabilised laser that is locked to a rubidium cell as shown in Fig. 4.5. The absorption spectrum of rubidium could be observed from the detector and the laser is locked to one of the atomic transitions.

780nm laser is coupled into the cavity via a 780nm compatible EEOM. A RF output signal generator is used to modify the frequency of the sideband produced by EEOM. With the laser locked to a transition in the the rubidium absorption spectrum, the frequency of the sideband is sitted on the peak of the transition (with its transmission intensity at the maximum) and is monitored

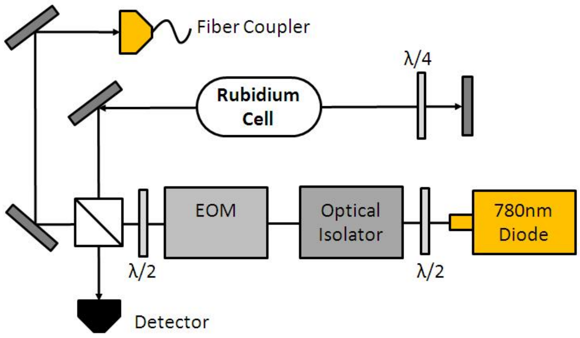

Figure 4.5: Schematic of the 780nm laser setup. The 780nm laser is locked to a rubidium reference and the laser is coupled into a fiber, which is then coupled into the cavity.

periodically. Drifts in the cavity will result in decrease in the intensity of the transmission signal observed, which can be compensated by changing the frequency of the sideband such that it is back on resonance with the cavity.

Chapter 5

Results and Discussions

With the equipment set up as mentioned in the previous chapter, measurements on the 650nm and 986nm beam properties were made through a high finesse cavity. This is to investigate if the objective to achieve the requirements as mentioned in the theoretical derivation in Chapter 2 are met. The beam properties would be presented and discussed.

5.1 Cavity Stability

Measurement for the drift of the cavity was taken over a period of a couple of hours using a 780nm laser locked to a rubidium reference. The laser is assumed to be not fluctuating in frequency. Any drifts observed would therefore be due to the drift in cavity resonance.

Over the hours that the readings for the drift of the cavity is taken, most short term fluctuations are observed in the order of about 0.5MHz in the first two hours of measurement. The overall largest drift was less than 2MHz too. We are more concerned about the short term drift of the cavity

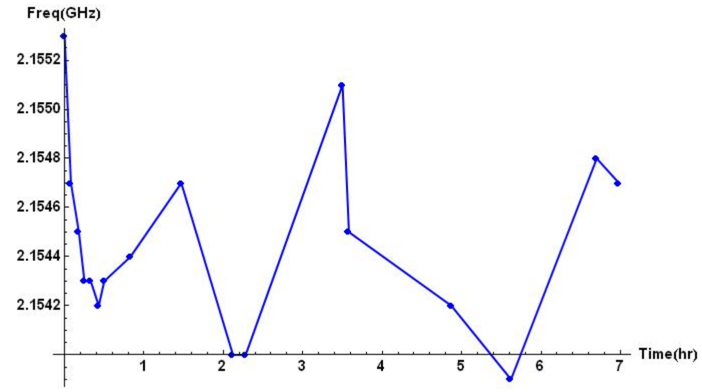

Figure 5.1: Plot of the frequency of the sideband generated from EEOM against time. The drift of the cavity is found be to less than 1.5MHz over the period of 7 hours. Drift of the cavity over a short period of an hour is found to be less than 0.5MHz.

because we want the absolute frequency difference to be stable over the course of the experiment. The stability on the long run assures us that the cavity is probably responding very slowly to the change in temperature of the lab, meaning that our isolation of cavity is working. Using Eq. 3.6, we would obtained the fluctuation of the absolute frequency difference to be less than 200kHz. This matches our tolerance of an absolute frequency difference fluctuation of about 200kHz.

Large fluctuations (of up to 2MHz) to the cavity frequency were attributed to the sudden change in temperature in the laboratory when the air-conditioning system dumps large amounts of cold air into the laboratory. This could cause one-off jump in the cavity frequency. However, since we are really interested in just the short term drift of the cavity, this effect is not too worrying. This suggests that we might have to re-calibrate our lasers frequency every half hour or so in such an event during the experiment, otherwise the drift is not of much concern.

5.2 650nm Laser Linewidth

The 650nm laser is operating at about 649.9nm, with a current supply of about 28.8mA and voltage supply of 15V. The temperature of the diode is maintained at about -15^{o}C. The operating parameters may be changed if necessary to tune the frequency of the laser and also to prevent the laser from mode-hopping.

The 650nm laser is coupled into a 650nm compatible EEOM. The output from the EEOM is coupled into a high finesse cavity for investigations on the linewidth of the laser. The EEOM is powered by a RF signal generator and the frequency of the sideband generated by the EEOM could be changed via the signal generator. Firstly, we investigate the linewidth of the high finesse cavity at 650nm.

The frequency output by the signal generator is a sine wave with amplitude 200kHz. The output of this sine wave is put into the trigger port of the digital scope, therefore the time domain of the digital scope could be sync to that of the generator.

$$f = 200 \sin(\omega t + \phi) \tag{5.1}$$

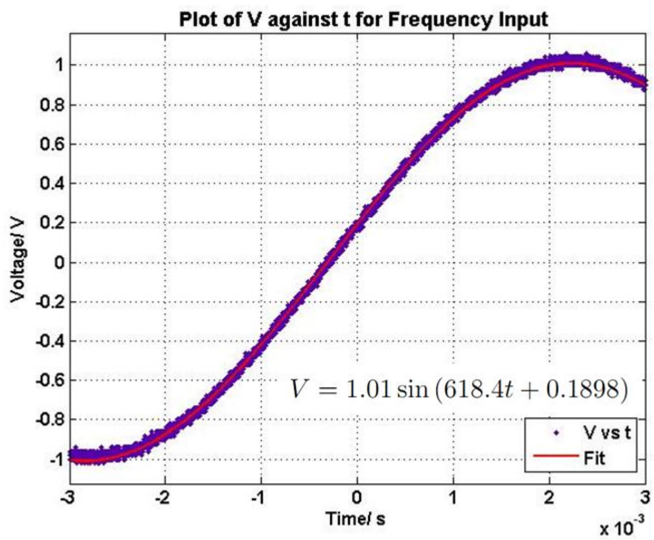

Figure 5.2: Plot of the voltage output of the signal to the time scale of the scope. The time scale of the scope is also the time scale of the sine wave generated by the signal generator, enabling us to obtain a value $\omega = 618.4$.

The time division in Fig. 5.2 is found to have negative values but that is not a cause for concern.

We can always view it as a linear shift to centre the axis. From the fit of the sine curve to the signal observed on the digital scope (refer Fig. 5.2), $\omega = 618.4$. This implies that the frequency sweep of amplitude 200kHz by the signal generator happens at a rate of $\omega = 618.4$.

The sideband of the 650nm laser is being scanned by the EEOM until it latches onto resonance with the cavity. The signal of the Lorentzian is being recorded by the digital scope and its full width at half maximum (FWHM), which translate to the cavity linewidth at 650nm, can be found by converting the time scale of the digital scope to the frequency domain.

$$\begin{aligned} \Delta f &= \frac{df}{dt}\Delta t \\ &= 200\,(\omega)\,cos\,(\omega t)\,\Delta t \\ &= 200 \times \omega \times \Delta t \end{aligned} \tag{5.2}$$

Here we have made the assumption that $\cos(\omega t) = 1$ because the Lorentzian peak would be sitting at the steepest slope of the sine wave, therefore the argument has to be an integer multiple of 2π. Having found out the value of ω from the curve fitting of the sine wave signal, we need to find out the time division that represents the FWHM. The cavity signal is fitted to a Lorentzian profile.

From the curve fitting, the FWHM in time domain is $\Delta t = 3.941 \times 10^{-4}$. Putting this into Eq. 5.2, the cavity linewidth (at FWHM) is found to be $f_c = 48.7kHz$.

With the cavity linewdith at 50kHz, the very clean signal of the 650nm laser suggests that the laser linewidth is much smaller than 50kHz. Now that the cavity linewidth at 650nm known, we proceed on to find the linewidth of the laser. We reduce the scanning range of the laser and zoom in on the steepest slope of the Lorentzian cavity signal, which is at the middle. The noise seen on the digital scope can be attributed to the noise of the laser, which is its linewidth. Firstly, we want to determine at which point of the slope the scope was sitting on. This is because the conversion

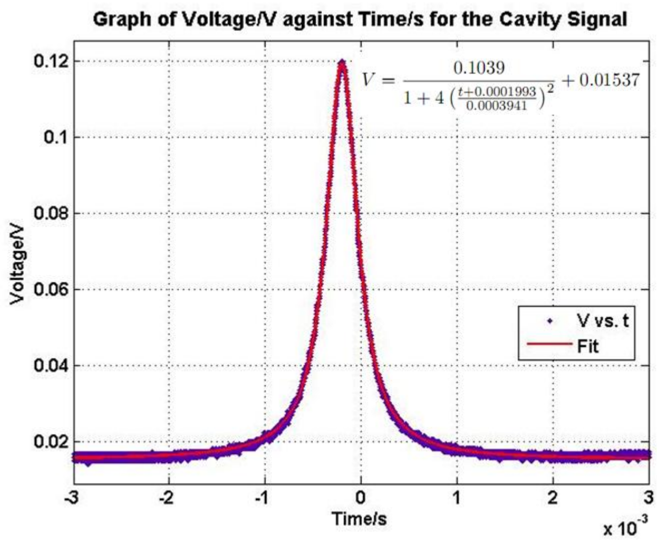

Figure 5.3: Plot of the voltage output of the cavity to the time scale of the scope. The FWHM in time domain of the scope can be found through the fit equation and it can be converted to frequency domain.

of the noise to frequency domain is not constant since the slope of the Lorentzian is not linear.

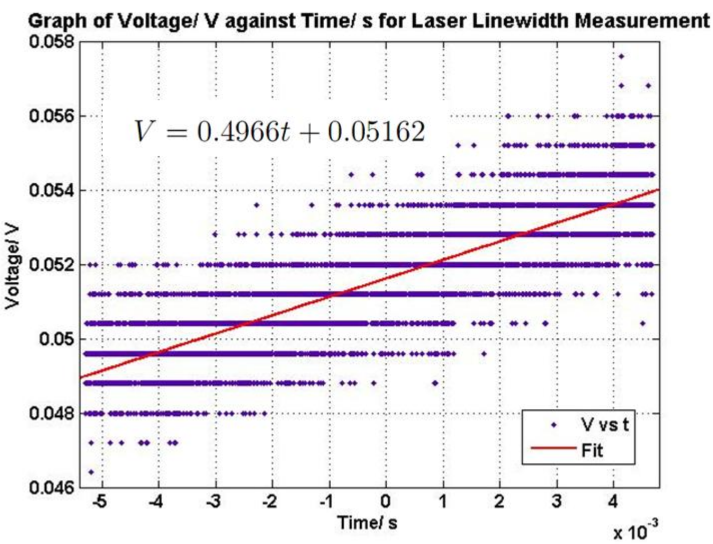

Figure 5.4: Plot of the voltage fluctuation due to laser linewdith to the time scale of the scope. The RMS error of the noise can be calculated and converted to FHWM of the laser linewidth.

The best fit line is noted to be slanted. This is due to the drift of the high finesse cavity because the high finesse cavity was not being temperature stabilised. However, it is not a cause of concern because we are mainly interested in the root mean square (RMS) error of the noise, which could then be converted to the FWHM of the laser signal, which is the laser linewidth.

As the slope of the Lorentzian is know to be increasing until the mid-point before decreasing to the peak, it is logical and convenient for us to choose the mid-point (x-axis) for our measurement. The expression for the Lorentzian of the cavity signal is as follows, as found from the fit (refer Fig. 5.3). The 'x-axis' is replaced with frequency, and the scaling factor has been dropped out for simplification with no loss of generality.

$$V = \frac{0.1039}{1 + 4\left(\frac{f}{f_c}\right)^2} + 0.01537 \tag{5.3}$$

Since the reading on the digital scope was taken at $V = 0.05162$ as found from the fit of the noise, by Eq. 5.3, $f = 33.2643$. This value of f is simply how far away from the peak (where $f = 0$) the reading was when it was taken. By taking the derivative of Eq. 5.3, we obtain the following.

$$\begin{aligned} \frac{dV}{df} &= \frac{8 \times 0.1039}{f_c} \times \frac{\frac{f}{f_c}}{\left(1 + 4\left(\frac{f}{f_c}\right)^2\right)^2} \\ &= 0.00142 \end{aligned} \tag{5.4}$$

The RMS error of the plot with respect to the best fit line is found to be $\Delta V_{RMS} = 8.976 \times 10^{-4}$. The linewidth of the laser can therefore be calculated as follows.

$$\begin{aligned} \Delta f &= \left(\frac{dV}{df}\right)^{-1} \Delta V_{RMS} \times 2.35 \\ &= 1.5 \end{aligned} \tag{5.5}$$

The linewidth of the 650nm laser is therefore calculated to be about 1.5kHz.

From the transmission signal observed through the high finesse cavity, the 650nm laser is seen to have a clean Lorentzian signal. This gives us extra confidence on our measurement of the linewidth. With the high finesse cavity having a narrow linewidth of about 50kHz, such a clean signal would imply that the linewidth of the laser has to be much smaller than 50kHz. This agrees with the narrow linewidth of the laser calculated from the noise in the spectrum.

This measurement provides encouraging results as we are able to achieve a linewidth of less than 20kHz, which was what we wanted to obtain when we started out. This would effectively reduce the jitter in the phase of the laser and increase the raman transfer efficiency.

5.3 986nm Laser Linewidth

The 986nm laser is obtained from a grating stabilised diode in a Toptica laser system that utilises digital locking. The laser is coupled into the cavity through a EEOM and is locked to the sideband generated by the EEOM. This allows tunability of the laser while staying on lock. The frequency of the sideband could be finetuned to acheive the required absolute frequency. The very same laser, through another path, is being frequency doubled by a non-linear crystal to obtain 493nm. This 493nm laser is then coupled into a optic fibre for shelving purposes.

In a similar treatment as that for 650nm, the 493nm laser was coupled into the high finesse cavity. The frequency of the 493nm laser can be changed accordingly by changing the frequency of the sideband of the 986nm laser, which is locked to the main cavity via the 780nm-compatible EEOM.

The scanning deviation used for investigating the 493nm laser is a frequency of amplitude 100kHz. Therefore, the frequency input for the sine wave could be modelled as follows.

$$f = 100 \sin(\omega t + \phi) \tag{5.6}$$

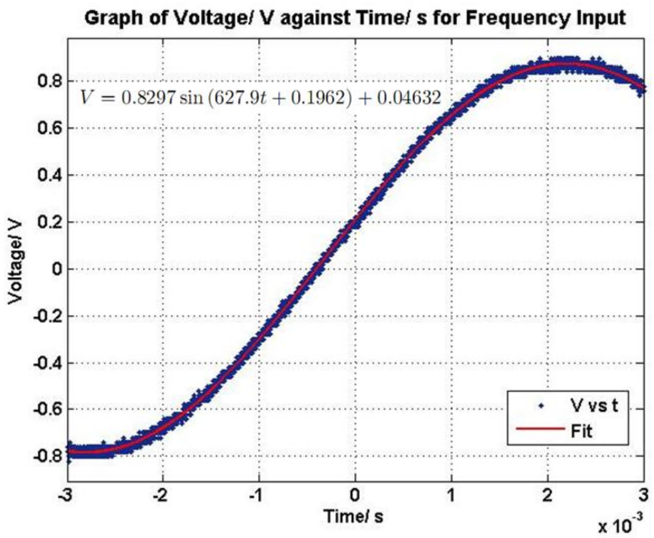

Figure 5.5: Plot of the voltage output of the signal to the time scale of the scope. The time scale of the scope is also the time scale of the sine wave generated by the signal generator, enabling us to obtain a value $\omega = 627.9$.

From the fit of the sine wave, we obtain $\omega = 627.9$.

The FWHM of the signal in time domain is found from the Lorentz fit to be $\Delta t = 3.25 \times 10^{-4}$.

$$\begin{aligned}\Delta f &= \frac{df}{dt}\Delta t \\ &= 100\,(\omega)\,cos\,(\omega t)\,\Delta t \\ &= 100 \times \omega \times \Delta t \\ &= 20.4\end{aligned} \tag{5.7}$$

At 493nm, the linewidth of the cavity $f_c = 20.4kHz$.

Similarly, we try to express the Lorentzian of the cavity signal (in voltage) as a function frequency.

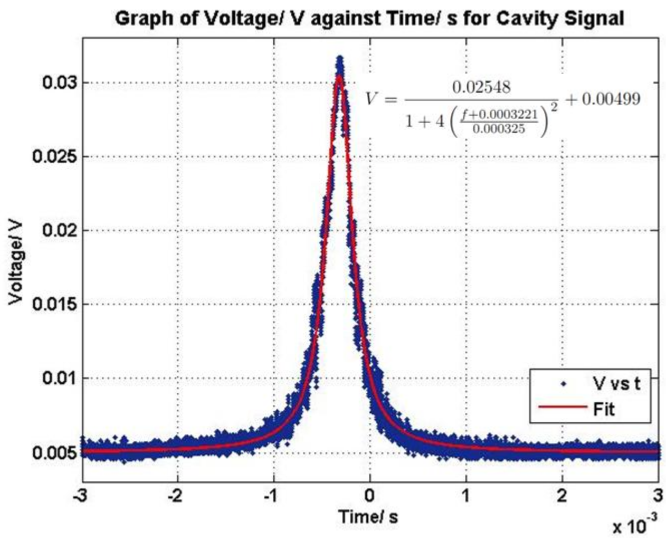

Figure 5.6: Plot of the voltage output of the cavity to the time scale of the scope. The FWHM in time domain of the scope can be found through the fit equation and it can be converted to frequency domain.

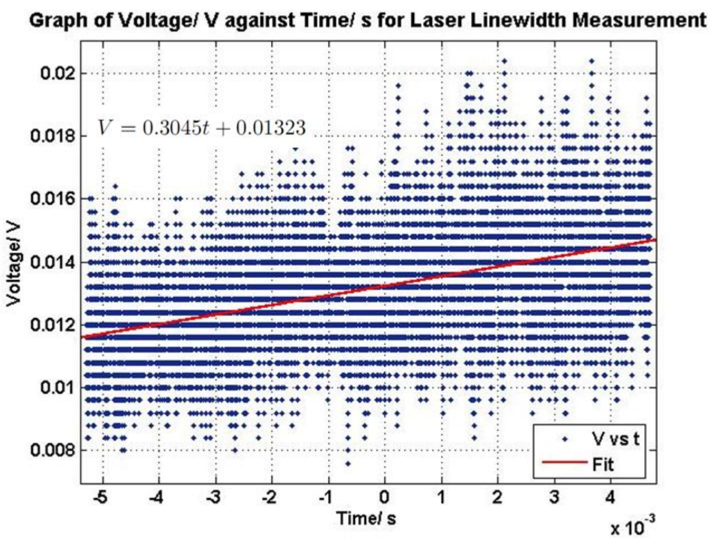

Figure 5.7: Plot of the voltage fluctuation due to laser linewdith to the time scale of the scope. The RMS error of the noise can be calculated and converted to FHWM of the laser linewidth.

$$V = \frac{0.02548}{1 + 4\left(\frac{f}{f_c}\right)^2} + 0.00499 \tag{5.8}$$

Since the reading on the digital scope was taken at $V = 0.01323$ as found from the fit of the noise, by Eq. 5.8, $f = 14.7538$. By taking the derivative of Eq. 5.8, we obtain the following.

$$\begin{aligned} \frac{dV}{df} &= \frac{8 \times 0.02548}{f_c} \times \frac{\frac{f}{f_c}}{\left(1 + 4\left(\frac{f}{f_c}\right)^2\right)^2} \\ &= 0.000756 \end{aligned} \tag{5.9}$$

The RMS error of the plot with respect to the best fit line is found to be $\Delta V_{RMS} = 1.685 \times 10^{-3}$. The linewidth of the laser can therefore be calculated as follows.

$$\begin{aligned} \Delta f &= \left(\frac{dV}{df}\right)^{-1} \Delta V_{RMS} \times 2.35 \\ &= 5.2 \end{aligned} \tag{5.10}$$

The linewidth of the 493nm laser is therefore calculated to be about 5.2kHz.

The linewidth of the laser is well within our requirement of at most 20kHz.

5.4 Transfer Efficiency

With an absolute frequency stability of about 200kHz, by solving Eq. 2.4, we would be able to obtain a transfer efficiency of $(99.0 \pm 0.9)\%$.

From the results for the 650nm and the 986nm lasers, both obtaining a laser linewidth of the order of 1kHz, we are confident that there would be high raman transfer efficiency based on our calculations. Assuming that we are able to maintain the absolute frequency requirement for the experiment (i.e. $\delta = 0$), by solving Eq. 2.5, we would be able to obtain a transfer efficiency of

$(99.8 \pm 0.2)\%$.

Chapter 6

Conclusions

We set off in this project wanting to build a laser system for the raman transition that shelves ions from $|F = 1, M_F = 1\rangle$ to $|F'' = 3, M''_F = 3\rangle$. This is part of an ion trap experiment, and it serves the purpose of a quantum state readout. To understand the challenges of this laser system, we look into the rabi flopping rate of the effective two level system and identified the absolute frequency fluctuations and the laser linewidth as major areas on concern which could decrease the coherence transfer efficiency.

Next, we draft out the requirements of the lasers by analysing the optical bloch equations for a three level system. The analysis reveals the need for the absolute frequency fluctuation to be within 200kHz and the average linewidth of the lasers to be less than 20kHz. In order to achieve these conditions, we couple the 650nm and 986nm lasers into a cavity. This cavity acts as a frequency selection to obtain the absolute frequency and also a frequency filter for the external cavity feedback technique.

The cavity is being stabilised to 1MHz over a period of an hour, which could effectively stabilise the absolute frequency of the lasers to about 200kHz. The heating strips attached to the vacuum chamber are able to maintain the temperature of the chamber at approximately $27^{o}C$, taking out the slow drift of the temperature of the laboratory. The foam and the plastic caps on the vacuum window takes out the fast change in the laboratory temperature, therefore maintaining the length of the cavity. With the cavity placed in a vacuum chamber, eliminating the change in refractive index of medium due to change in temperature, the optical path length of the cavity is well stabilised.

The external cavity feedback technique is able to narrow the linewidth of the lasers to the order of 1kHz. These results are very favourable and could possibly bring the transfer efficiency of the shelving process to higher than 99%.

The laser beam parameters for both 650nm and 493nm are found to be within the required stability and linewidth based on our calculations for a 99% population transfer in the shelving process. However, the raman lasers were not able to be tested for their state transfer efficiency in the laboratory. The imaging system is required to be set up to measure the fluorescence and process is undergoing.

Appendix A

Rabi Frequency

To obtain the rabi frequency for the raman transition, firstly, we need to obtain the dipole matrix element for the relevant transitions. The table below gives us the wavelengths of the transitions, their respective branching ratios, the dipole matrix elements and their decay rates.

Transition	$\lambda\,(nm)$	$A/2\pi\,(MHz)$	$\mu\,\left(\times 10^{-29}Cm\right)$	p
$S_{1/2} \leftrightarrow P_{1/2}$	493.5453	15.427	2.03	0.745
$D_{3/2} \leftrightarrow P_{1/2}$	649.8692	5.276	1.80	0.255

Table A.1: Tabulation of the wavelengths of the transitions (λ), their respective branching ratios (p), the dipole matrix elements (μ) and their decay rates (A).

The dipole matrix elements tabulated in the table could be calculated using the Einstein A coefficient, which relates the dipole matrix elements to their Clebsch-Gordon coefficient and decay rates.

$$A = \frac{\omega_0^3 \mu^2}{3\pi\epsilon_0 \hbar c^3} \tag{A.1}$$

With reference to the derivations presented by D. J. Wineland *et al.* 2003 [5], g_b and g_r are defined to be

$$\begin{aligned} g_k &= \frac{\mu_k E_{0k}}{\hbar} \\ &= \frac{\mu_k}{\hbar}\sqrt{\frac{2I_k}{\epsilon_0 c}} \qquad \text{since} \quad E_{0k}^2 = \frac{2I_k}{\epsilon_0 c} \end{aligned} \tag{A.2}$$

The rabi rate is given by

$$\Omega_R = \frac{\mu_b \mu_r}{2\Delta}\frac{2\sqrt{I_b I_r}}{\epsilon_0 c}\left(\frac{1}{2}\times\frac{1}{\sqrt{3}}\right) \tag{A.3}$$

Here, the factor of $\frac{1}{\sqrt{3}}$ arises due to the coupling coefficient of $|F'' = 3, M_F'' = 3\rangle$ and $|F' = 2, M_F' = 2\rangle$ while the factor of $\frac{1}{2}$ arises due to the coupling of the blue laser between $|F = 1, M_F = 1\rangle$ and $|F' = 2, M_F' = 2\rangle$. Similar beam paraters that minimises the effects of stark shifts are chosen as per mentioned in the article.

The net stark shift of the kth beam on the m_s electronic level, where the kth beam refers to the blue and the red lasers; the m_s level refers to $|F = 1, M_F = 1\rangle$ and $|F'' = 3, M_F'' = 3\rangle$, is given by

$$\delta\left(m_s, k\right) = \frac{1}{4\hbar^2}\frac{2I_k\mu^2}{\epsilon_0 c}c_k^2 \tag{A.4}$$

c_k is the coupling coefficient between the respective levels. It is therefore possible to obtain the same stark shifts for both states by choosing the appropiate beam intensity having the ratio

$$\begin{aligned} \frac{\mu_b^2 I_b}{3} &= \frac{\mu_r^2 I_r}{4} \\ \frac{I_b}{I_r} &\approx 0.59 \end{aligned} \tag{A.5}$$

With the above mentioned beam parameters requirements, for a 650nm laser with power of 5mW, 493nm laser with 1.5mW, both having a beam waist of about 30μm, and a detuning of 80GHz from the $P_{1/2}$ state, we obtain a rabi frequency of about 2MHz for the raman transition.

Appendix B

Elimination of Excited States

The three level system shown in Fig. 2.1 can be reduced to a two level system due to the large detuning of the raman beams from the $P_{1/2}$ state. Here, we show the details of the reduction of the three level system. Below are the optical bloch equations that define the three level Λ system. The $S_{1/2}$, $D_{3/2}$ and $P_{1/2}$ states are refered to as state 1, 2 and 3 respectively.

$$\dot{\rho}_{33} = -\Gamma\rho_{33} - i\left(\rho_{13} - \rho_{31}\right)\frac{\Omega_1}{2} - i\left(\rho_{23} - \rho_{32}\right)\frac{\Omega_2}{2} \tag{B.1}$$

$$\dot{\rho}_{11} = \Gamma_1\rho_{33} + i\left(\rho_{13} - \rho_{31}\right)\frac{\Omega_1}{2} \tag{B.2}$$

$$\dot{\rho}_{22} = \Gamma_2\rho_{33} + i\left(\rho_{23} - \rho_{32}\right)\frac{\Omega_2}{2} \tag{B.3}$$

$$\dot{\rho}_{13} = \left(-\Gamma_{13} - i\Delta_1\right)\rho_{13} - i\left(\rho_{33} - \rho_{11}\right)\frac{\Omega_1}{2} + i\rho_{12}\frac{\Omega_2}{2} \tag{B.4}$$

$$\dot{\rho}_{23} = \left(-\Gamma_{23} - i\Delta_2\right)\rho_{23} - i\left(\rho_{33} - \rho_{22}\right)\frac{\Omega_2}{2} + i\rho_{21}\frac{\Omega_1}{2} \tag{B.5}$$

$$\dot{\rho}_{12} = i\left(\Delta_2 - \Delta 1\right)\rho_{12} + i\rho_{13}\frac{\Omega_2}{2} - i\rho_{32}\frac{\Omega_1}{2} - \gamma\rho_{12} \tag{B.6}$$

where Ω_1 and Ω_2 are the rabi frequencies of the lasers coupling the $S_{1/2} - P_{1/2}$ and $D_{3/2} - P_{1/2}$ transitions respectively. Δ_1 and Δ_2 are the detuning of the laser beams from the resonance of $S_{1/2} - P_{1/2}$ and $D_{3/2} - P_{1/2}$ transitions. Γ is the decay rate of the $P_{1/2}$ state, Γ_1 and Γ_2 are the decay rates of $Gamma_{13}$, Γ_{23} and $\Gamma_{12} \equiv \gamma$. The laser linewidth of the 650nm and 493nm lasers are denoted by γ_2 and γ_1. The coherence decay rates are given by

$$\Gamma_{13} = \left(\Gamma + \gamma_1\right)/2 \tag{B.7}$$

$$\Gamma_{23} = \left(\Gamma + \gamma_2\right)/2 \tag{B.8}$$

$$\gamma = \left(\gamma_1 + \gamma_2\right)/2 \tag{B.9}$$

A simplifying assumption that $\Gamma_{13} = \Gamma_{23}$ would be made since the laser linewdith are small compared to Γ and are approximately equal in our case [6].

To carry out the elimination of the excited state, the following assumptions were made. These assumptions are valid because we expect the population of the excited state, ρ_{33}, to be very small compared to the other states.

$$\dot{\rho}_{13} = \dot{\rho}_{23} = \dot{\rho}_{33} = 0 \tag{B.10}$$

$$\rho_{33} << \rho_{11} \tag{B.11}$$

$$\rho_{33} << \rho_{22} \tag{B.12}$$

Combining Eq. B.10, B.11 and B.12 with Eq. B.1, B.4 and B.5, we obtain the following expressions.

$$\begin{aligned} \rho_{13} &= \frac{-i\left(\rho_{33}-\rho_{11}\right)\frac{\Omega_1}{2} + i\rho_{12}\frac{\Omega_2}{2}}{\Gamma_{13}+i\Delta_1} \\ &\approx \frac{i\rho_{11}\frac{\Omega_1}{2} + i\rho_{12}\frac{\Omega_2}{2}}{\Gamma_{13}+i\Delta_1} \end{aligned} \tag{B.13}$$

$$\begin{aligned} \rho_{23} &= \frac{-i\left(\rho_{33}-\rho_{22}\right)\frac{\Omega_2}{2} + i\rho_{21}\frac{\Omega_1}{2}}{\Gamma_{23}+i\Delta_2} \\ &\approx \frac{i\rho_{22}\frac{\Omega_2}{2} + i\rho_{21}\frac{\Omega_1}{2}}{\Gamma_{23}+i\Delta_2} \end{aligned} \tag{B.14}$$

Substituting Eq. B.13, B.14 and B.10 into Eq. B.1, we obtain

$$\rho_{33} = \frac{-i\left(\rho_{13}-\rho_{31}\right)\frac{\Omega_1}{2} - i\left(\rho_{23}-\rho_{32}\right)\frac{\Omega_2}{2}}{\Gamma} \tag{B.15}$$

Since $\rho_{13} = \rho_{31}^{\dagger}$ and $\rho_{23} = \rho_{32}^{\dagger}$, let us at this point evaluate $(\rho_{13} - \rho_{31})$ and $(\rho_{23} - \rho_{32})$. We attempt to express the the density matrix differential equation in terms of ρ_{11}, ρ_{22}, ρ_{12} and c.c.

$$\begin{aligned} \left(\rho_{13}-\rho_{31}\right) &= \frac{i\rho_{11}\frac{\Omega_1}{2} + i\rho_{12}\frac{\Omega_2}{2}}{\Gamma_{13}+i\Delta_1} - \frac{-i\rho_{11}\frac{\Omega_1}{2} - i\rho_{21}\frac{\Omega_2}{2}}{\Gamma_{13}-i\Delta_1} \\ &= \frac{i\rho_{11}\Omega_1\Gamma_{13} + i\frac{\Omega_2}{2}\Gamma_{13}\left(\rho_{12}+\rho_{21}\right) + \frac{1}{2}\Omega_2\Delta_1\left(\rho_{12}-\rho_{21}\right)}{{\Gamma_{13}}^2 + {\Delta_1}^2} \end{aligned} \tag{B.16}$$

$$\begin{aligned}
(\rho_{23}-\rho_{32}) &= \frac{i\rho_{22}\frac{\Omega_2}{2}+i\rho_{21}\frac{\Omega_1}{2}}{\Gamma_{23}+i\Delta_2}-\frac{-i\rho_{22}\frac{\Omega_2}{2}-i\rho_{12}\frac{\Omega_1}{2}}{\Gamma_{23}-i\Delta_2} \\
&= \frac{i\rho_{22}\Omega_2\Gamma_{23}+i\frac{\Omega_1}{2}\Gamma_{23}(\rho_{12}+\rho_{21})-\frac{1}{2}\Omega_1\Delta_2(\rho_{12}-\rho_{21})}{{\Gamma_{23}}^2+{\Delta_2}^2}
\end{aligned} \tag{B.17}$$

Putting Eq. B.15, B.16 and B.17 into Eq. B.2, B.3 and B.6, we obtain the following terms. Until this point, the equations are very general and valid with minimal assumptions made. Here, we define a new quantity $\Omega_R=\frac{\Omega_1\Omega_2}{2\Delta_1}$.

$$\begin{aligned}
\dot{\rho}_{11} &= \Gamma_1\rho_{33}+i(\rho_{13}-\rho_{31})\frac{\Omega_1}{2} \\
&= \frac{\Gamma_1}{\Gamma}\left(-i\frac{\Omega_1}{2}(\rho_{13}-\rho_{31})-i\frac{\Omega_2}{2}(\rho_{23}-\rho_{32})\right)+i\frac{\Omega_1}{2}(\rho_{13}-\rho_{31}) \\
&= \frac{\Gamma_2}{2\Gamma}\frac{-\rho_{11}\Gamma_{13}\left(\frac{\Omega_1}{\Delta_1}\right)^2-\frac{\Omega_1\Omega_2}{2{\Delta_1}^2}\Gamma_{13}(\rho_{12}+\rho_{21})+i\frac{\Omega_1\Omega_2}{2\Delta_1}(\rho_{12}-\rho_{21})}{\left(\frac{\Gamma_{13}}{\Delta_1}\right)^2+1} \\
&\quad+\frac{\Gamma_1}{2\Gamma}\frac{\rho_{22}\Gamma_{23}\left(\frac{\Omega_2}{\Delta_2}\right)^2+\frac{\Omega_1\Omega_2}{2{\Delta_2}^2}\Gamma_{23}(\rho_{12}+\rho_{21})+i\frac{\Omega_1\Omega_2}{2\Delta_2}(\rho_{12}-\rho_{21})}{\left(\frac{\Gamma_{23}}{\Delta_2}\right)^2+1} \\
&= \frac{\frac{-\Gamma_{13}\Gamma_2}{\Gamma}\left(\frac{\Omega_1}{4\Delta_1}\right)^2}{\left(\frac{\Gamma_{13}}{\Delta_1}\right)^2+1}\rho_{11}+\frac{\frac{\Gamma_{23}\Gamma_1}{\Gamma}\left(\frac{\Omega_2}{4\Delta_2}\right)^2}{\left(\frac{\Gamma_{23}}{\Delta_2}\right)^2+1}\rho_{22} \\
&\quad+\frac{i}{2}\frac{\Omega_R}{\left(\frac{\Gamma_{13}}{\Delta_1}\right)^2+1}(\rho_{12}-\rho_{21})+\Gamma_{13}\left(\frac{\Gamma_1}{\Gamma}-1\right)\frac{\frac{\Omega_1\Omega_2}{2\Delta_1^2}}{\left(\frac{\Gamma_{13}}{\Delta_1}\right)^2+1}(\rho_{12}+\rho_{21})
\end{aligned} \tag{B.18}$$

The first term $(\frac{\Omega_1^2}{4\Delta_1^2})$ can be interpreted as the scattering of the laser beam , resulting in the optical pumping of the population in state 1 to state 2, explaining the negative sign in the term. The second term can be seen as the 'spontaneous emission' term in a two level system, which is actually also due to the scattering of laser in this case. The third term can be interpreted as the effective rabi flopping between states 1 and 2, with the effective rabi rate Ω_R.

In the regime of weak probe intensity and large detuning, the following assumptions are made to simplify the expression.

$$\Delta^2 >> \Gamma_{13}^2, \Gamma_{23}^2 \tag{B.19}$$

$$\begin{aligned} \Omega_1^2 &<< \Delta_1^2 \\ \Omega_2^2 &<< \Delta_2^2 \end{aligned} \tag{B.20}$$

Using the very same argument, the same steps could be performed to the expression of $\dot{\rho}_{22}$. The expression for $\dot{\rho}_{11}$ and $\dot{\rho}_{22}$ simplifies to the following neat expressions.

$$\dot{\rho}_{11} = -i\frac{\Omega_R}{2}\left(\rho_{21} - \rho_{12}\right) \tag{B.21}$$

$$\dot{\rho}_{22} = i\frac{\Omega_R}{2}\left(\rho_{21} - \rho_{12}\right) \tag{B.22}$$

The expression for the coherence term is as follow

$$\begin{aligned} \dot{\rho}_{12} &= i\left(\Delta_2 - \Delta 1\right)\rho_{12} + i\rho_{13}\frac{\Omega_2}{2} - i\rho_{32}\frac{\Omega_1}{2} - \gamma\rho_{12} \\ &= -\left(\gamma + i\delta\right)\rho_{12} + \frac{i}{2}\frac{i\rho_{11}\frac{\Omega_1\Omega_2}{2} + \rho_{12}\frac{\Omega_2{}^2}{2}}{\Gamma_{13} + i\Delta_1} - \frac{i}{2}\frac{-i\rho_{22}\frac{\Omega_1\Omega_2}{2} - i\rho_{12}\frac{\Omega_1{}^2}{2}}{\Gamma_{23} - i\Delta_2} \\ &= -\left(\gamma + i\delta\right)\rho_{12} + \frac{-\Gamma_{13}\frac{\Omega_R}{2\Delta_1}\rho_{11} + \frac{i}{2}\Omega_R\rho_{11} - \Gamma_{13}\frac{\Omega_2^2}{4\Delta_1^2}\rho_{12} + i\frac{\Omega_2^2}{4\Delta_1}\rho_{12}}{\left(\frac{\Gamma_{13}}{\Delta_1}\right)^2 + 1} \\ &\quad + \frac{-\Gamma_{23}\frac{\Omega_R}{2\Delta_2}\rho_{22} - \frac{i}{2}\Omega_R\rho_{22} - \Gamma_{23}\frac{\Omega_1^2}{4\Delta_2^2}\rho_{21} + i\frac{\Omega_1^2}{4\Delta_2}\rho_{21}}{\left(\frac{\Gamma_{23}}{\Delta_2}\right)^2 + 1} \\ &\approx -\left(\gamma + i\delta\right)\rho_{12} + i\frac{\Omega_R}{2}\left(\rho_{11} - \rho_{22}\right) \end{aligned} \tag{B.23}$$

The above simplified equations can be expressed in matrix form, where we will further analysis would be carried out. In our derivation, we have assumed with no loss of generality that the rabi frequency term is real. The time derivative of the equation is scaled by a factor of Ω_R for simplification, with $\tau = \Omega_R t$.

$$\frac{d}{d\tau}\begin{pmatrix}\rho_{11}\\ \rho_{22}\\ \rho_{12}\\ \rho_{21}\end{pmatrix} = \frac{i}{2}\begin{pmatrix}0 & 0 & 1 & -1\\ 0 & 0 & -1 & 1\\ 1 & -1 & \frac{2}{\Omega_R}(i\gamma-\delta) & 0\\ -1 & 1 & 0 & \frac{2}{\Omega_R}(i\gamma+\delta)\end{pmatrix}\begin{pmatrix}\rho_{11}\\ \rho_{22}\\ \rho_{12}\\ \rho_{21}\end{pmatrix} \tag{B.24}$$

B.1 Absolute Frequency Requirement

Here, we want to investigate the effect of the detuning in absolute frequency on the transfer efficiency from the ground state, therefore we assume the laser linewidth $\gamma = 0$. Using the bloch sphere picture, we want to express the set of differential equations in u, v and w. Let

$$\begin{aligned} u =& \rho_{11} - \rho_{22} \\ v =& i\left(\rho_{21} - \rho_{12}\right) \\ w =& \rho_{21} + \rho_{12} \end{aligned} \tag{B.25}$$

By simple differentiation and substitution,

$$\begin{aligned} \frac{du}{d\tau} &= \frac{d\rho_{11}}{d\tau} - \frac{d\rho_{22}}{d\tau} \\ &= \frac{i}{2}\left(\rho_{12} - \rho_{21}\right) - \frac{i}{2}\left(\rho_{21} - \rho_{12}\right) \\ &= i\left(\rho_{12} - \rho_{21}\right) \\ &= -v \end{aligned} \tag{B.26}$$

$$\begin{aligned}\frac{dv}{d\tau} &= i\left(\frac{d\rho_{21}}{d\tau} - \frac{d\rho_{12}}{d\tau}\right)\\ &= (\rho_{11} - \rho_{22}) - \frac{\delta}{\Omega_R}(\rho_{21} + \rho_{12})\\ &= u - \frac{\delta}{\Omega_R}w\end{aligned} \tag{B.27}$$

$$\begin{aligned}\frac{dw}{d\tau} &= \frac{d\rho_{21}}{d\tau} + \frac{d\rho_{12}}{d\tau}\\ &= i\frac{\delta}{\Omega_R}(\rho_{21} - \rho_{12})\\ &= \frac{\delta}{\Omega_R}v\end{aligned} \tag{B.28}$$

Here, we define $\beta = \frac{\delta}{\Omega_R}$. We rearrange the above equations to decouple the differential equation.

$$\ddot{v} + \left(1 + \beta^2\right)v = 0 \tag{B.29}$$

Solving for the second order differential equation, we obtain a solution v. The solution is found with the initial conditions that all the population is in the lower state, thus $u(0) = 1$, $v(0) = 0$ and $\dot{v}(0) = 1$.

$$v = -\frac{i}{2\sqrt{1+\beta^2}}\left(e^{i\sqrt{1+\beta^2}\tau} - e^{-i\sqrt{1+\beta^2}\tau}\right) \tag{B.30}$$

Using Eq. B.26, we solve for u, with the same initial conditions, and express ρ_{22} as a function of β and τ, via the relationship that $\rho_{11} + \rho_{22} = 1$ and the definition of u.

$$\begin{aligned}u &= -\frac{1}{2(1+\beta^2)}\left(e^{i\sqrt{1+\beta^2}\tau} - e^{-i\sqrt{1+\beta^2}\tau}\right) + \frac{\beta}{1+\beta^2}\\ &= \frac{1}{1+\beta^2}\left(cos\left(\sqrt{1+\beta^2}\tau\right) + \beta^2\right)\end{aligned} \tag{B.31}$$

$$
\begin{aligned}
\rho_{22} &= \frac{1}{2}(1-u) \\
&= \frac{1}{2(1+\beta^2)}\left(1 - cos\left(\sqrt{1+\beta^2}\tau\right)\right) \\
&= \frac{1}{4}\frac{sin^2\left(\frac{\sqrt{1+\beta^2}}{2}\tau\right)}{\frac{1+\beta^2}{4}}
\end{aligned}
\tag{B.32}
$$

The value of β is solved for $\rho_{22} = 0.99$ and $\tau = \pi$, since we want a 99% transfer efficiency using a π-pulse. The value obtained for beta is $\beta = 0.100$, which means that the detuning from the absolute frequency can only be 10% of the rabi frequency. With a rabi frequency of about 2MHz, we would require the laser stability to be within 200kHz over the experiment.

B.2 Laser Linewidth Requirement

In a similar fashion as the treatment in the previous section, we want to investigate the effects of the laser linewidth on the transfer efficiency, therefore, we set the absolute frequency detuning $\delta = 0$. Expressing the density matrix using the bloch sphere representation Eq. 2.3,

$$
\begin{aligned}
\frac{du}{d\tau} &= \frac{d\rho_{11}}{d\tau} - \frac{d\rho_{22}}{d\tau} \\
&= \frac{i}{2}(\rho_{12} - \rho_{21}) - \frac{i}{2}(\rho_{21} - \rho_{12}) \\
&= i(\rho_{12} - \rho_{21}) \\
&= -v
\end{aligned}
\tag{B.33}
$$

$$
\begin{aligned}
\frac{dv}{d\tau} &= i\left(\frac{d\rho_{21}}{d\tau} - \frac{d\rho_{12}}{d\tau}\right) \\
&= (\rho_{11} - \rho_{22}) - i\frac{\gamma}{\Omega_R}(\rho_{21} - \rho_{12}) \\
&= u - \frac{\gamma}{\Omega_R}v
\end{aligned}
\tag{B.34}
$$

$$\begin{aligned}
\frac{dw}{d\tau} &= \frac{d\rho_{21}}{d\tau} + \frac{d\rho_{12}}{d\tau} \\
&= -\frac{\gamma}{\Omega_R}\left(\rho_{21} + \rho_{12}\right) \\
&= -\frac{\gamma}{\Omega_R} w
\end{aligned} \tag{B.35}$$

The first two equations can be decoupled easily to form a second order differential equation.

$$\ddot{u} + \frac{\gamma}{\Omega_R}\dot{u} + u = 0 \tag{B.36}$$

We want to find an analytical solution to u, so as to understand the population in state 2. Using the initial conditions that $u(0) = 1$, $v(0) = 0$ and $\dot{v}(0) = 1$, which implies that at $\tau = 0$, only state 1 is populated, we are able to obtain a solution to u. Here we define $\alpha = \frac{\gamma}{\Omega_R}$.

$$\begin{aligned}
u &= Ae^{i\lambda_1 \tau} + Be^{i\lambda_2 \tau} \\
\lambda_1 &= \frac{i}{2}\alpha + \sqrt{1 - \frac{\alpha^2}{4}} \\
\lambda_2 &= \frac{i}{2}\alpha - \sqrt{1 - \frac{\alpha^2}{4}} \\
A &= \frac{1}{2} - \frac{i\alpha}{2\sqrt{4 - \alpha^2}} \\
B &= \frac{1}{2} + \frac{i\alpha}{2\sqrt{4 - \alpha^2}}
\end{aligned} \tag{B.37}$$

Using the relationship that $u = \rho_{11} - \rho_{22}$ and the normalisation that $\rho_{11} + \rho_{22} = 1$, we choose to extract the real part of the solution of u and express ρ_{22} in terms of α and τ.

$$\begin{aligned}
\rho_{22} &= \frac{1}{2}\left(1 - u\right) \\
&= \frac{1}{2}\left(1 - e^{-\frac{\alpha\tau}{2}} cos\left(\sqrt{1 - \frac{\alpha^2}{4}}\tau\right)\right) \\
&= \frac{1}{2}\left(1 - e^{-\frac{\gamma t}{2}} cos\left(\sqrt{\Omega_R^2 - \frac{\gamma^2}{4}}t\right)\right)
\end{aligned} \tag{B.38}$$

The value of alpha is solved for $\rho_{22} = 0.99$ and $\tau = \pi$ since we want a 99% transfer efficiency using a π-pulse. The value obtained for alpha is $\alpha = 0.0129$ using Mathematica, which means that the linewidth has to be within 1.3% of the rabi frequency. With a rabi frequency of about 2MHz, the average linewidth can only be about 20kHz.

Appendix C

Experimental Setup

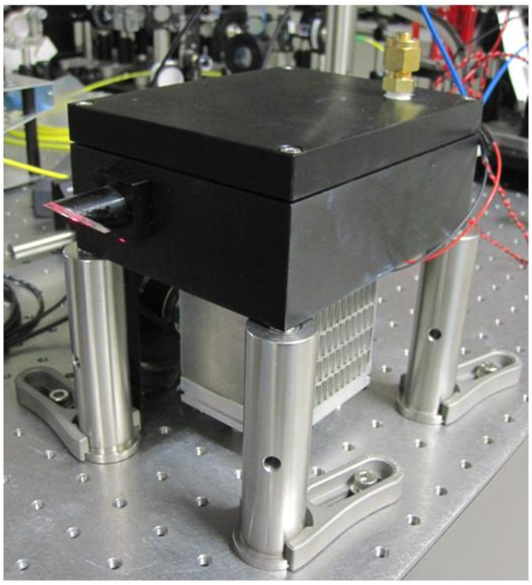

Figure C.1: The diode housing has a heat sink with fins attached below. The cooler fan that runs at 12V can be seen behind the diode, aiding in the dissipation of heat from the heat sink to the surrounding. The fan is placed on rubber dampers to reduce the mechanical noise on the table.

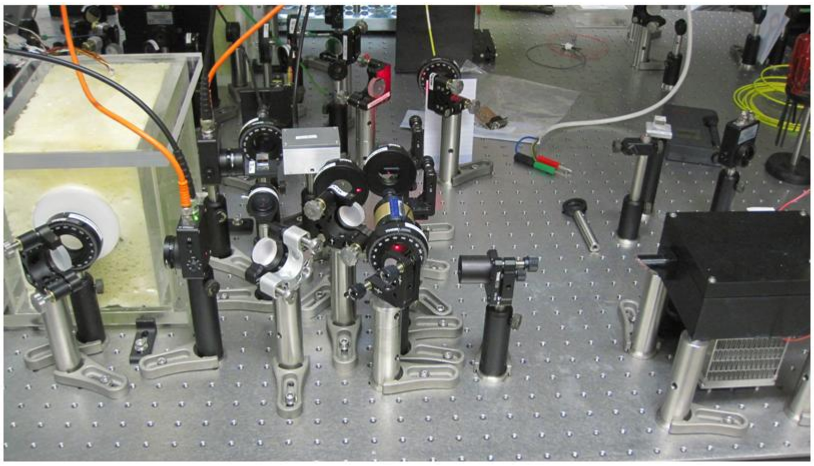

Figure C.2: The experimental setup for the 650nm laser. The diode housing is placed further away from the set up so that the fan does not introduce unwanted air flow to the setup. Laser from the 650nm diode is coupled to the cavity and feedbacked to the diode.

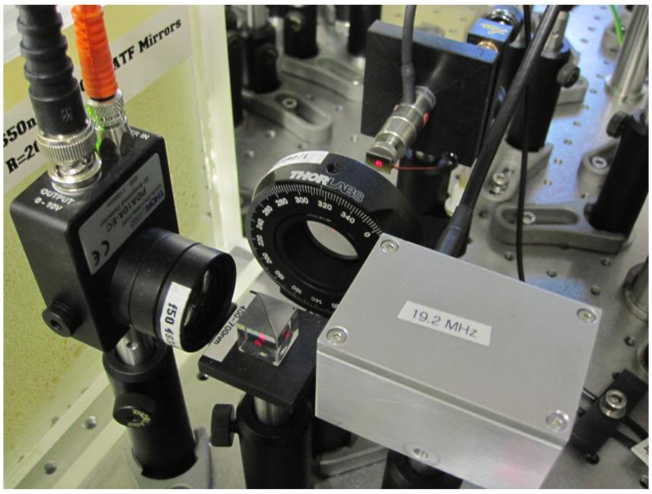

Figure C.3: A mirror is mounted on the PZT, which is attached to an actuator. The EOM puts sidebands of 19.2MHz on the laser and the reflected signal goes into the PDA-10 detector via the PBS. The signal is then fed to a lock-in circuit that controls the voltage output on the PZT, therefore maintaining the lock of the laser.

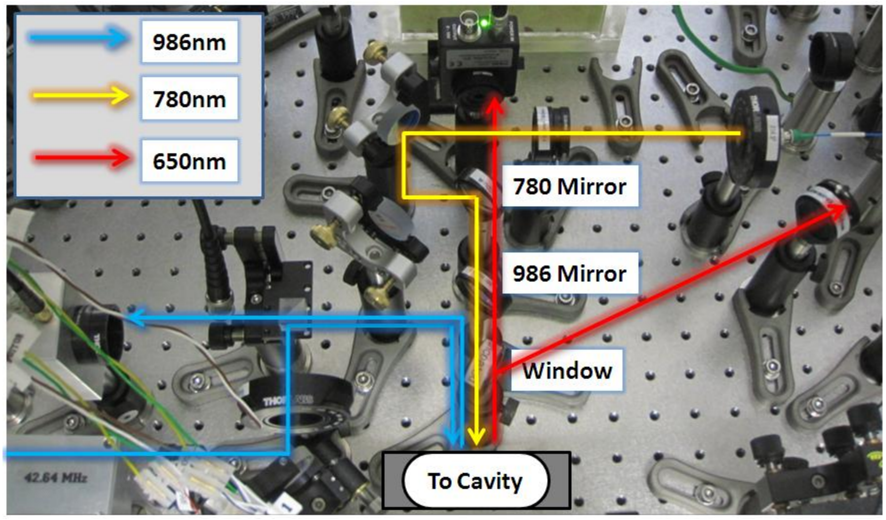

Figure C.4: Setup at the 'rear' of the cavity. 650nm laser is reflected off the window and feed-backed to the diode for the external cavity locking technique. The transmitted beam is put into a photodetector to observe the transmission signal. The 986nm laser is coupled into the cavity and a PDH lock is set up. 780nm laser could be coupled into the cavity to understand the drift of the cavity. Both the 650nm and 780nm have relatively high transmission ratio through the 986 mirror.

Reference

[1] R. Blatt and G. Werth, Phys. Rev. A **25**, 1476 (1982)

[2] Ralph G. Devoe and Christian Kurtsiefer, Phys. Rev. A **65**, 063407 (2002).

[3] K. P. Birch and M. J. Downs, Metrologia **31**, 315-316 (1994)

[4] D. J. Wineland, C. Monroe, W. M. Itano, D. Leibfried, B. E. King and D. M. Meekhof, J. Res. Natl. Inst. Stand. Technol. 103, 259 (1998)

[5] D. J. Wineland, M.Barrett, J. Britton, J. Chiaverini, D. DeMarco, W. M. Itano, B. Jelenkovic, C. Langer, D. Leibfried, W. Meyer, T. Rosenband and T. Schatz, R. Soc. Lond. A **361**, 1349-1361 (2003)

[6] M. J. McDonnel, D. N. Stacey and A. M. Steane, Phys. Rev. A **70**, 053802 (2004)

[7] P. Villemoes, A. Arnesen, F. Heijkenskjold and A. Wannstrom, J. Phys. B 26, 4289 (1993)

[8] A. S. Arnold, J. S. Wilson and M. G. Boshier, Rev. Sci. Instrum. **69**, 3 (1998)

[9] B. Dahmani, L. Hollberg and R. Drullinger, Opt. Lett. **12**, 11 (1987)

[10] PH. Laurent, A. Clairon and CH. Breant, IEEE J. Quantum Electronics **25**, 6 (1989)

[11] E. D. Black, Am. J. Phys. **69**, 1 (2001)

[12] K. P. Birch and P. T. Wilton, Appl. Opt. **27**, 14 (1988)

[13] L. Davidovich, M. Orszag and N. Zagury, Phys. Rev. A **54**, 6 (1996)

[14] Harold J. Metcalf, Peter van der Straten, *Laser Cooling and Trapping*, (Springer, 1999).